Creld2 function during unfolded protein response is essential for liver metabolism homeostasis

Paul Kern[1,5], Nora R. Balzer[1], Franziska Bender[5], Alex Frolov[1], Jan-Peter Sowa[6,7], Lorenzo Bonaguro[2,5], Thomas Ulas[2,4], Christoph Thiele[3], Joachim L. Schultze[2,4], Ali Canbay[6,7], Reinhard Bauer[5], Elvira Mass[1]*

1 Developmental Biology of the Immune System, Life & Medical Sciences (LIMES) Institute, University of Bonn, 53115 Bonn, Germany

2 Genomics and Immunoregulation, Life & Medical Sciences (LIMES) Institute, University of Bonn, 53115 Bonn, Germany

3 Biochemistry & Cell Biology of Lipids, Life & Medical Sciences (LIMES) Institute, University of Bonn, 53115 Bonn, Germany

4 Platform for Single Cell Genomics and Epigenomics at the German Center for Neurodegenerative Diseases and the University of Bonn, 53127 Bonn, Germany

5 Developmental Genetics & Molecular Physiology, Life & Medical Sciences (LIMES) Institute, University of Bonn, 53115 Bonn, Germany

6 Department of Gastroenterology, Hepatology and Infectious Diseases, University Hospital Magdeburg, 39120 Magdeburg, Germany

7 Department of Medicine, Ruhr University Bochum, University Hospital Knappschaftskrankenhaus Bochum, 44892 Bochum, Germany

*corresponding author: emass@uni-bonn.de

Abstract

The unfolded protein response (UPR) is associated with the hepatic metabolic function, yet it is not well understood how endoplasmic reticulum (ER) disturbance might influence metabolic homeostasis. Here, we describe the physiological function of Cysteine-rich with EGF-like domains 2 (Creld2), previously characterized as a downstream target of the ER-stress signal transducer Atf6. Creld2 enhances protein folding and degradation through its interaction with proteins involved in UPR, thereby, promoting tolerance of chronic stress and recovery from acute stress. *Creld2*-deficiency leads to a dysregulated UPR, and causes the development of hepatic steatosis in male mice, while females are protected. We observed this sex dimorphism also in humans with fatty liver disease, with only males showing an accumulation of CRELD2 protein in the liver. These results reveal a Creld2 function at the intersection between UPR and metabolic homeostasis and suggest a mechanism in which chronic ER stress underlies fatty liver disease in males.

Introduction

The Cysteine-rich with EGF-like domains (Creld) protein family consists of two members – Creld1 and Creld2 – and is highly conserved across species [1,2]. The domain structure between these proteins is almost identical with the only difference of transmembrane domains being present in Creld1, but lacking in Creld2 [3]. This leads to the distinct localization and functions of these proteins within a cell: Creld1 is proposed to be anchored in the endoplasmic reticulum (ER) membrane with its domains facing the cytoplasm [4], although a plasma membrane bound form facing the extracellular matrix has been predicted as well [1]. We previously characterized the function of Creld1 being essential for heart development in mice [4]. Creld2 is localized predominantly within the ER, can be secreted [3], and has been characterized as a

53 marker for kidney disease in urine [5] and for prosthetic joint infections in synovial fluid
54 [6]. However, the physiological role of Creld2 *in vivo* remains unknown.

55 Several *in vitro* studies have identified Creld2 as an ER-stress inducible gene,
56 whose expression is regulated by activating transcription factor 6 (Atf6) [7,8]. ER stress
57 is characterized by an accumulation of proteins in the ER lumen. Consequently, cells
58 activate an unfolded protein response (UPR), a signaling network that collectively aims
59 at decreasing ER protein load by broad inhibition of protein synthesis and at the same
60 time promotes the activation and production of proteins that increase protein folding
61 capacity and degradation. The latter include chaperones, shuttling proteins that
62 promote secretion of proteins out of the ER and ER-associated protein degradation
63 (ERAD) components [9].

64 The UPR is controlled by three sensors: Atf6, inositol requiring enzyme 1 (Ire1),
65 and protein kinase RNA-activated (PKR)-like ER kinase (Perk). The ER luminal
66 domains of the ER stress sensors are bound and thereby inactivated by the chaperone
67 Grp78 (glucose-regulated protein 78, also known as heat shock protein A5 (Hspa5)).
68 Upon ER stress Grp78 is sequestered by the accumulation of proteins in the ER lumen,
69 causing the activation of the three sensors. Perk dimerizes and is activated by trans-
70 autophosphorylation of its kinase domains, leading to translational inhibition through
71 eIF2a phosphorylation. This directly enhances the translation of DNA-damage-
72 inducible 34 (Gadd34) and CAAT/enhancer-binding protein (C/EBP) homologous
73 protein (Chop). While Gadd34 serves as a feedback loop to dephosphorylate eIF2α
74 allowing the cell to recover from translational inhibition, increased Chop expression
75 may trigger cell death due to unresolved ER stress. The kinase Ire1 undergoes
76 autophosphorylation resulting in splicing of the *X-box binding protein 1* (*sXbp1*) mRNA
77 producing an active transcription factor, which induces the transcription of chaperones
78 and ERAD pathway components. ER-membrane bound Atf6 is cleaved and

79 translocates to the nucleus where it activates target genes including ERAD
80 components, chaperones, and phospholipid synthesis [10].

81 The liver is a highly secretory organ and serves frequently as the tissue to study
82 ER stress. Using genetic and dietary models of obesity, a link between hepatic stress
83 and insulin resistance has been established [11–14], suggesting that the accumulation of
84 lipids within hepatocytes and the resulting hepatocellular damage is linked to
85 dysfunction of the ER. On the contrary, chemically induced UPR leads to hepatic
86 steatosis through the direct and indirect regulation of lipid metabolism [15–17], leaving the
87 arrow of causality between hepatosteatosis and UPR unclear.

88 Here, we generated a *Creld2* knockout mouse to address Creld2 protein
89 function during steady state, and dissect its role during UPR and diet-induced obesity
90 in the liver. We show that *Creld2* deficiency promotes the development of liver
91 steatosis in male mice, and identify Creld2 interaction partners that are involved in ER-
92 stress release, thereby placing Creld2 functionally into the cellular stress response of
93 a cell *in vivo*. The conserved function of Creld2 across species is supported by the
94 accumulation of CRELD2 in male patients with non-alcoholic steatohepatitis (NASH).

95

96 **Results**

97 Aged *Creld2*$^{eGFP/eGFP}$ males develop hepatic steatosis

98 To investigate Creld2 function *in vivo* we generated a *Creld2*-knockout mouse model
99 by replacing the endogenous locus with an enhanced green fluorescent protein (eGFP)
100 (*Creld2*$^{eGFP/eGFP}$, Figure S1A), allowing the use of both *Creld2*$^{WT/eGFP}$ *and*
101 *Creld2*$^{eGFP/eGFP}$ as reporter mice for *Creld2* expression. We confirmed ubiquitous
102 protein expression [18] as well as lack of Creld2 expression in *Creld2*$^{eGFP/eGFP}$ mice in
103 various tissues via Western blot (Figure S1B). *Creld2*$^{eGFP/eGFP}$ mice were born in
104 Mendelian ratios (Figure 1A) and were viable. Young mice (1-2 month-old) did not

105 show any differences in body weight (Figure 1B), organ development or changes in
106 tissue morphology as assessed histologically in the liver, pancreas, and muscle (Figure
107 S1C, and not shown).

108 We next assessed body and organ weights of ~1-year-old mice (12-15 months).
109 We observed that the body and liver weight of *Creld2*$^{eGFP/eGFP}$ mice was lower than that
110 of *Creld2*$^{WT/WT}$ controls (Figure 1B, C). We first performed hematoxylin/eosin (HE) and
111 Masson Goldner Trichrome (MGT) stainings to investigate pathophysiological changes
112 in the liver. While MGT staining did not reveal a fibrotic phenotype (Figure S1D-E),
113 *Creld2*$^{eGFP/eGFP}$ animals presented with dilated sinusoids and abundant vacuoles in
114 hepatocytes indicating a metabolic dysregulation of the liver (Figure 1D). To investigate
115 whether *Creld2*$^{eGFP/eGFP}$ livers store increased amounts of glycogen or lipids, we
116 performed Periodic Acid-Schiff (PAS) and Oil-red-O (ORO) stainings, respectively. The
117 glycogen content was not altered (Figure S1D, E), but ORO staining indicated that
118 *Creld2*$^{eGFP/eGFP}$ livers contain more neutral lipids compared to *Creld2*$^{WT/WT}$ controls
119 (Figure 1D). Glutamine synthetase (GS) expression in liver parenchyma is typically
120 restricted to pericentral hepatocytes, however, under high-fat diet conditions GS
121 expression is upregulated and can be found outside hepatocytes lining the central
122 veins [19]. Therefore, we assessed GS expression as an indicator of dysregulated
123 metabolism. Indeed, *Creld2*$^{eGFP/eGFP}$ livers showed ectopic expression of GS, while
124 control livers showed immunoreactivity only in pericentral hepatocytes, as expected
125 (Figure 1D).

126 To analyse the hepatic neutral lipid composition quantitatively, we performed
127 thin layer chromatography and observed that *Creld2*$^{eGFP/eGFP}$ livers accumulate more
128 free fatty acids (FFA), diacylglycerols (DAG), cholesterol, and cholesteryl esters,
129 whereas triacylglycerols (TAG) remain at similar levels as in *Creld2*$^{WT/WT}$ livers (Figure
130 1E). Intriguingly, we noticed that liver pathology was absent in 1-year-old females (not

131 shown) and lipid content analysis confirmed that *Creld2*$^{eGFP/eGFP}$ females were
132 protected from the development of a hepatosteatotic phenotype (Figure 1E).
133 Our finding that old *Creld2*$^{eGFP/eGFP}$ males developed hepatosteatosis prompted
134 us to perform glucose and insulin tolerance tests to assess their glucose homeostasis.
135 Injection of glucose tendentially led to an augmented blood glucose level response in
136 *Creld2*$^{eGFP/eGFP}$ males after 15-30 minutes when compared to control littermates
137 (Figure 1F). Correspondingly, *Creld2*$^{eGFP/eGFP}$ mice were unable to respond as well as
138 *Creld2*$^{WT/WT}$ mice to an injection of insulin, with a maximum drop of blood glucose levels
139 to ~80 %, while wildtype controls reduced their blood glucose to ~60 % of the starting
140 value (Figure 1G).
141 Increased blood glucose concentrations after insulin and glucose injection as
142 well as abundant DAG levels are indicative for hepatic insulin resistance caused by
143 impaired insulin signalling at the level of the insulin receptor kinase [20,21]. To investigate
144 whether *Creld2*$^{eGFP/eGFP}$ mice suffer from hepatic insulin resistance, we analysed livers
145 for phosphorylation of Akt as a proxy for active insulin signalling. Yet, *Creld2*$^{eGFP/eGFP}$
146 livers displayed rather elevated pAkt/Akt ratios 15 min after insulin injection in
147 comparison to *Creld2*$^{WT/WT}$ mice (Figure 1H), indicating an intact hepatic insulin
148 receptor signalling. In summary, our data suggest that *Creld2* deficiency causes
149 hepatic steatosis during ageing in male mice without driving hepatic insulin resistance
150 or overall obesity.
151
152 <u>Aged *Creld2*$^{eGFP/eGFP}$ males downregulate key mediators of lipid homeostasis in the</u>
153 <u>liver but show no acute ER stress or inflammatory response</u>
154 To investigate the underlying molecular mechanisms leading to lipid accumulation in
155 *Creld2*$^{eGFP/eGFP}$ livers, we performed qRT-PCR analyses on key mediators of lipid
156 homeostasis. We observed that genes encoding the transcription factor *Pgc1*α

157 (*Ppargc1a*), components of fatty acid oxidation (*Acox1*), acylglycerol metabolism
158 (*Apoc2, Dgat1, Dgat2*) and cholesterol storage (*Apob100, Lsr*) were downregulated in
159 livers of *Creld2*$^{eGFP/eGFP}$ males compared to controls (Figure 2A, Table S1).

160 We next assessed whether *Creld2*$^{eGFP/eGFP}$ livers experience increased ER
161 stress due to the accumulation of lipids by analysing the expression of chaperones
162 *Grp78* (*Hspa5*), *Grp94* (*Hsp90b1*) and the apoptosis inducer *Chop* (*Ddit3*). All three
163 markers showed increased expression on a transcriptional level, indicating ongoing
164 UPR (Figure 2B, Table S1). Albeit not significant, *Creld2*$^{eGFP/eGFP}$ livers also presented
165 with higher Grp78 and Chop protein levels when compared to littermate controls
166 (Figure 2C, S1F). Thus, we analysed whether these changes led to activation of the
167 three UPR axes Atf6, Ire1 and Perk. Neither *Edem1* and *Derl3* as part of the ERAD
168 machinery and downstream targets of Atf6 [22], nor *Ire1* (*Ern1*) and *sXbp1* as part of the
169 Ire1 pathway showed significant differences in gene expression in male *Creld2*$^{eGFP/eGFP}$
170 mice compared to controls (Figure 2B). Activation of the Perk pathway was determined
171 through the phosphorylation status of Perk and eIF2 as well as by protein expression
172 of Gadd34. We observed increased phosphorylation of PERK suggesting that
173 *Creld2*$^{eGFP/eGFP}$ livers experience ER stress, however, the signalling downstream of
174 PERK was not altered when compared to controls (Figure 2C). In line with the lack of
175 hepatosteatosis, livers of female *Creld2*$^{eGFP/eGFP}$ mice did not show major
176 transcriptional alterations in UPR or lipid metabolism pathways (Figure S2A-C).

177 Next, we addressed whether increasing levels of inflammation and tissue
178 damage, which are the basis for the progression of non-alcoholic fatty liver disease
179 (NAFLD) to non-alcoholic steatohepatitis (NASH), could be the leading cause of the
180 dysregulated metabolism. Intriguingly, qRT-PCR of pro-inflammatory cytokines (*Il1b,*
181 *Il6, Tnfa*) and acute phase response genes (*Apcs, Saa3*) revealed an overall
182 downregulation of these genes in *Creld2*$^{eGFP/eGFP}$ livers when compared to *Creld2*$^{WT/WT}$

183 (Figure 2D, Table S1). Under steady state, tissue-resident macrophages, also called
184 Kupffer cells, are the main cytokine-producing cells in the liver. However, comparison
185 of their numbers revealed that *Creld2*$^{eGFP/eGFP}$ livers harbor rather more Kupffer cells
186 (Figure S2D), suggesting that the reduction of cytokine expression was not due to
187 reduced Kupffer cell numbers.

188 During inflammatory conditions such as hepatosteatosis, monocytes are
189 recruited to the liver where they differentiate into macrophages and become a source
190 of pro-inflammatory cytokines [23]. To test whether *Creld2* deficiency affected the
191 production of cytokines by monocyte-derived macrophages, bone-marrow derived
192 macrophages (BMDMs) of 1-year-old male mice were treated with lipopolysaccharide
193 (LPS) and the expression of *Tnfa*, *Il1b* and *Il6* was assessed after 4 h and 8 h of LPS
194 treatment (Figure S2E). Both *Creld2*$^{eGFP/eGFP}$ and *Creld2*$^{WT/WT}$ controls showed peaking
195 cytokine gene expression after 4 h, with decreasing expression levels at 8 h of LPS
196 stimulation, but no differences in transcript levels between both genotypes was
197 observed (Figure S2E). Taken together, *Creld2*-deficiency does not lead to severe
198 UPR or directly affects the immunological response. Instead, lack of Creld2 function
199 during steady state results in a subthreshold ER stress and decreased expression of
200 genes essential for lipid homeostasis, thereby evoking increased lipid storage in 1-
201 year-old *Creld2*$^{eGFP/eGFP}$ males.

202

203 *Impaired cell survival in Creld2-deficient cells upon chronic ER stress*

204 To better characterize a possible role of Creld2 in UPR we turned to an *in vitro* system
205 and treated mouse embryonic fibroblasts (MEFs) from wildtype and *Creld2*$^{eGFP/eGFP}$
206 animals with increasing concentrations of the ER stress inducing agents tunicamycin
207 (Tm, 25–100 ng/ml) and thapsigargin (Tg, 2.5–10 nM) [24]. Untreated knockout cells
208 expanded similarly to wildtype MEFs, indicating that Creld2 is not required for cell

209 proliferation under steady state conditions (Figure 3A). Cell numbers of wildtype MEFs
210 increased at low concentrations or remained stable at higher concentrations of Tm and
211 Tg. However, *Creld2*-deficient MEFs were unable to cope with the induced stresses as
212 evidenced by reduced cell numbers after 3 days Tm treatment or 2 days Tg treatment,
213 independent of the dosage (Figure 3A). To test whether *Creld2*-deficient MEFs showed
214 a differential response to chronic ER stress we challenged the cells with the highest
215 concentrations of Tm (100 ng/ml) and Tg (10 nM) and analyzed UPR for up to 3 days
216 (Figure S3). Similar to wildtype controls, *Creld2*-deficient cells upregulated expression
217 of Grp78, Grp94 and Chop on transcriptional and protein levels (Figure S3A, B, I, Table
218 S2). Furthermore, responses in the Perk and Ire1a branches, as assessed by *Perk*
219 and *Gadd34* mRNA abundance, Gadd34 protein and P-eIF2a/eIF2a ratio as well as
220 expression of *Ire1a* and *sXbp1* transcripts, were comparable to controls (Figure S3C,
221 D, E, I).

222 Analysis of the Atf6 branch in *Creld2*$^{WT/WT}$ MEFs revealed that *Creld2* transcript
223 is highly upregulated after 24h of Tm and Tg (9 to 14-fold) and that protein levels
224 reached a 2-fold enrichment compared to steady state. However, *eGFP* expression in
225 *Creld2*$^{eGFP/eGFP}$ MEFs increased only ~2.5-fold on transcriptional level, and no change
226 in GFP protein levels could be detected (Figure S3F, G, I, Table S2), suggesting a
227 positive feedback loop for Creld2 expression during UPR in wildtype cells. Further, *Atf6*
228 expression was not altered in *Creld2*-deficient MEFs, however, the expression of Atf6
229 downstream targets *Edem1* and *Derl3* were downregulated throughout both the Tm
230 and Tg treatments in comparison to controls (Figure S3H, Table S2). Together, these
231 data suggested that Creld2 is indeed required for cell homeostasis and cell growth
232 under chronic ER stress conditions and that *Creld2*-deficiency may promote the
233 accumulation of misfolded glycoproteins, as the induction of ERAD-associated genes
234 *Edem1* and *Derl3* was suppressed in *Creld2*-knockout MEFs.

235 <u>*Diminished UPR and cell survival in Creld2-deficient cells during ER-stress recovery*</u>
236 Complementary to the chronic ER-stress model, we set out to establish an ER-stress
237 recovery model where MEFs were treated for a short period of time (1-8 hours) with a
238 high concentration of Tg and then let recover for 5 days to mimic rather physiological
239 stress conditions. Successful induction of UPR within these 8 h was monitored by the
240 expression of *Grp78*, *Chop*, *Atf6a*, *Perk*, *Ire1a* and downstream targets of the three
241 UPR axes (Figure S3J, Table S3). Already 2 h of Tg were sufficient to deteriorate the
242 survival of *Creld2*-knockout MEFs as evidenced by a significantly lower cell number
243 when compared to controls (Figure 3B). We therefore chose the 2 h time point to
244 investigate UPR during the 2-day recovery phase. To assess whether MEFs indeed
245 underwent UPR during the recovery phase, we first assessed the expression of
246 general ER-stress markers Grp78, Grp94 and Chop (Figure 3C, Table S4). *Grp78* and
247 *Chop* expression peaked at 10 h, with significantly less production of *Grp78* in
248 *Creld2*$^{eGFP/eGFP}$ MEFs at later time points (Figure 3C, Table S4). *Grp94* expression
249 peaked at 30 h, however, *Creld2*-knockout MEFs showed a suppressed induction
250 throughout the recovery phase in comparison to controls (Figure 3C, Table S4). In
251 concordance with gene expression, Grp78 protein accumulated in both genotypes in
252 the beginning of the recovery phase (10 h), and increased even further at 30 h and 48
253 h albeit transcript levels declined (Figure 3C, D, S3K, Table S4). Similar to their gene
254 expression, Grp78 protein levels were lower in *Creld2*$^{eGFP/eGFP}$ MEFs compared to
255 wildtype controls during the recovery phase, while Chop was induced in a similar
256 manner in both genotypes (Figure 3D, Figure S3K). Together, these data hinted
257 towards an insufficient UPR in *Creld2*$^{eGFP/eGFP}$ MEFs, which prompted us to investigate
258 the activation of the three UPR axes.
259 *Atf6a* and *Edem1* expression were induced similarly in knockout and wildtype
260 cells, but *Derl3* expression was decreased in *Creld2*$^{eGFP/eGFP}$ MEFs (Figure 3E, Table

261 S4). In wildtype cells, *Creld2* mRNA expression was upregulated 6 h after Tg treatment
262 initiation and increased even further throughout the 2-day recovery phase with a peak
263 at 30 h (Figure 3E, Table S4). An accumulation of Creld2 protein was evident only after
264 30 h and increased even further after 48 h (Figure 3F, S3K). As a reporter for Creld2
265 expression we analyzed *eGFP* mRNA levels in *Creld2*$^{eGFP/eGFP}$ MEFs. Although *eGFP*
266 increased in a similar temporal manner the expression reached a maximum of ~3.5-
267 fold in comparison to the starting point, while the endogenous *Creld2* expression was
268 increased to ~16-fold (Figure 3E, Table S4), which is similar to what we observed
269 under chronic stress conditions.

270 To investigate Perk axis activation, we measured transcript levels of *Perk* and
271 *Gadd34* as well as phosphorylation of Perk and eIF2a proteins (Figure 3G, H, S3K,
272 Table S4). Although there was no difference on transcriptional level, with both *Perk*
273 and *Gadd34* being upregulated during the recovery phase (Figure 3G, Table S4),
274 *Creld2*-deficient MEFs displayed lower phosphorylation levels of Perk before and
275 during Tg treatment and the recovery phase (Figure 3H, S3K). Similarly, the P-
276 eIF2a/eIF2a ratio was diminished before ER-stress induction in *Creld2*$^{eGFP/eGFP}$ MEFs
277 in comparison to *Creld2*$^{WT/WT}$. During the recovery phase, *Creld2*$^{eGFP/eGFP}$ cells showed
278 a delayed phosphorylation of eIF2a with a peak after 30 h without reaching baseline
279 levels after 48 h, whereas *Creld2*$^{WT/WT}$ MEFs exhibited increasing P-eIF2/eIF2 ratios
280 until 10 h followed by a decrease to baseline values after 30 h (Figure 3H, S3K).

281 In the Ire1a branch, *Creld2*-deficient and wildtype MEFs showed a similar
282 behavior after the ER-stress challenge: both, *Ire1a* gene expression and splicing of
283 *Xbp1* (*sXbp1*) during the recovery phase was increased, and remained at high levels
284 after 48 h (Figure 3I, Table S4). In summary, our data indicate that UPR within the Atf6
285 and Perk axes is partially deteriorated or delayed in *Creld2*-deficient cells leading to
286 their diminished cell growth and increased apoptosis.

287 *Accumulation of lipids does not lead to UPR*

288 Given that Creld2 is required for a proper mounting of UPR and that aged
289 *Creld2*$^{eGFP/eGFP}$ mice develop hepatosteatosis and show elevated Grp78, Chop and P-
290 Perk protein levels, we next asked whether the prolonged accumulation of lipids
291 causes unresolved ER stress in these animals or vice versa. To induce the
292 development of fatty liver, we placed 8-week-old *Creld2*$^{eGFP/eGFP}$ males and wildtype
293 littermates on control diet (CD) or high-fat diet (HFD). To test whether animals could
294 recover from hepatosteatosis, we split the HFD group after 8 weeks with one group
295 remaining on HFD for 4 more weeks and one group that was switched to CD (HFD>CD,
296 Figure 4A). Supporting our findings in aged mice (Figure 1B), we found that
297 *Creld2*$^{eGFP/eGFP}$ animals on CD gained less weight over time (Figure 4B). Similarly, after
298 8-12 weeks on HFD *Creld2*$^{eGFP/eGFP}$ showed reduced bodyweights when compared to
299 littermate controls (Figure 4B), but still developed insulin resistance as measured by
300 the homeostatic model assessment indices of insulin resistance (HOMA-IR) (Figure
301 4C). Moreover, both genotypes increased the total tissue weight of livers and
302 epididymal white adipose tissue (eWAT) (Figure 4D) indicating that *Creld2*$^{eGFP/eGFP}$
303 animals were not protected from diet-induced obesity.

304 Histological assessment of the liver showed an increased ORO staining in HFD-
305 fed mice (Figure S4A, B), which was accompanied by a small decrease in PAS signal
306 (Figure S4C, D) confirming diet-induced hepatosteatosis in both genotypes.
307 Accumulation of lipids in general, which resulted mainly from TAG and DAG
308 accumulation, was confirmed by shotgun lipidomics (Figure 4E). *Creld2*$^{eGFP/eGFP}$ livers
309 contained generally less lipids (Figure 4E), which could account for the on average
310 lower liver weight (Figure 4B). HFD did not induce a fibrotic phenotype, nor did it affect
311 liver function as assessed by MGT staining (Figure S4E, F) and alanine
312 aminotransferase (ALT) concentrations in the serum (Figure S4G), respectively. When

313 the HFD groups where switched to CD, their body, liver and eWAT weight returned to
314 the level of animals that were kept on CD (Figure 4B, D). Further, ORO and PAS
315 signals as well as the amount of lipids normalized in both genotypes (Figure 4D, E,
316 S4A-D). Together, our data indicate that on organismal and tissue level *Creld2*-
317 deficient mice responded similarly to wildtype mice upon diet-induced obesity and lipid
318 uptake as well as mobilization of lipids after a diet switch from HFD to CD.

319 To test whether lipid accumulation or subsequent lipid mobilization triggered
320 differential cellular stress responses in *Creld2*$^{eGFP/eGFP}$ and littermate control livers, we
321 performed RNA-sequencing (RNA-seq) after 12 weeks on diet (Figure S4H). We made
322 use of Construction of Co-expression network analysis (CoCena) that clusters genes
323 into distinct modules based on the expression patterns across the two genotypes and
324 three conditions. CoCena identified a module (purple), which contains genes being
325 highly expressed after HFD>CD recovery, but which are also globally upregulated in
326 *Creld2*$^{eGFP/eGFP}$ livers when comparing them to *Creld2*$^{WT/WT}$ in each condition (Figure
327 4F, Table S5). Gene Ontology (GO) and Hallmark terms indicated that many of the
328 833 genes were involved in the regulation of fatty acid metabolic processes as well as
329 in the ERK signaling cascade. Among these genes were *Plin2*, which belongs to the
330 perilipin family and serves as a marker for lipid accumulation, as well as genes coding
331 for enzymes catalyzing the formation of distinct lipid species (*Acot2*, *Eci2*, *Chka*,
332 *Mogat1*, *Pnpla2*, *Elovl5*, *Pck1, Gpat3, Crot)*, lipid transfer and lipid uptake proteins
333 (*Tnfaip8l3*, *Scarb1*, *Sorl1*, *Lrp10*), and proteins regulating insulin signaling (*Irs1, Insig2,*
334 *Angptl4, Igfbp3, Cltrn, Slc16a1*) (Figure 4G). Many of these genes are correlated to
335 fatty acid oxidation and hepatic lipid mobilization, which may explain why
336 *Creld2*$^{eGFP/eGFP}$ livers show reduced lipid amounts as they upregulate these genes
337 even more than *Creld2*$^{WT/WT}$ after HFD>CD recovery. This is in contrast to what we
338 observed in aged mice, where enzymes such as *Acox1* and *Acot2* are downregulated

339 (Figure 2A), suggesting that Creld2 is not directly regulating metabolic gene
340 expression, similarly to what has been reported for *Atf6*-knockout mice [15].

341 Further, CoCena identified the royalblue module (63 genes) with globally
342 upregulated genes in *Creld2*$^{eGFP/eGFP}$ livers showing highest differences after CD and
343 HFD (Figure 4F). GO and Hallmark enrichment analyses indicated an enrichment for
344 mRNA processing and apoptosis. Additionally, the black module that showed an
345 induction of 126 genes in *Creld2*$^{eGFP/eGFP}$ livers after HFD also returned 'apoptosis' as
346 GO term suggesting that knockout livers may have increased mRNA levels and
347 undergo apoptosis due to unresolved ER stress. This notion was supported by an
348 increase of ceramides in *Creld2*$^{eGFP/eGFP}$ livers after HFD (Figure 4H), as their
349 accumulation has been associated to apoptosis in hepatosteatosis [25]. Indeed,
350 immunoblotting against cleaved Caspase3 confirmed that *Creld2*$^{eGFP/eGFP}$ livers after
351 HFD underwent increased apoptosis when compared to *Creld2*$^{WT/WT}$ (Figure 4I, S4H).

352 The module midnightblue identified 703 genes that were generally
353 downregulated in *Creld2*$^{eGFP/eGFP}$ livers when compared to controls, particularly after
354 the diet switch from HFD to CD, and that were involved in protein folding and long-
355 chain fatty acid metabolism based on GO enrichment analysis. Among these genes
356 were cytochrome p450 genes that oxidize polyunsaturated fatty acids (PUFA), which
357 may lead to an increase of lipotoxic ω-6 PUFA [26] in *Creld2*-deficient livers. Moreover,
358 chaperones and co-chaperones (*Hspa4l, Hsp90aa1, Fkbp4, Dnaja4, Unc45b, Hspa13,*
359 *Calr*) including *Hspa5* (*Grp78*) were downregulated (Figure 4G). We therefore
360 investigated whether Grp78 expression and UPR activation were affected on the
361 protein level. Yet, neither Grp78 nor phosphorylation levels of Perk and eIF2a were
362 significantly changed in *Creld2*$^{eGFP/eGFP}$ livers when compared to littermate controls,
363 (Figure 4J, S43H). Further, the comparison of CD versus HFD groups per genotype
364 did not reveal any sign of induced ER stress on transcript or protein level (Figure 4G,

365 J), with Grp78 and Chop expression being even downregulated after HFD when
366 compared to CD (Figure 4J). To test for other targets of the UPR that might be affected
367 by the dietary change and that may have not been included in the CoCena analysis,
368 we additionally performed a direct pairwise comparison of differentially expressed
369 genes between CD or HFD *Creld2*$^{WT/WT}$ or *Creld2*$^{eGFP/eGFP}$ animals. None of these
370 analyses returned genes involved in UPR (Table S6) indicating that 12 weeks of HFD
371 do not induce acute ER stress in the liver. Taken together, our data suggest that
372 *Creld2*$^{eGFP/eGFP}$ animals can generally cope with an excess of lipid uptake for a short
373 time period of 12 weeks, despite transcriptional changes that hint towards altered lipid
374 metabolic processes. Furthermore, neither transcriptome nor protein expression
375 analysis revealed a lipid-driven ER stress response in the liver, despite an enhanced
376 lipotoxicity phenotype in *Creld2*$^{eGFP/eGFP}$ mice.
377
378 *Unresolved ER stress perturbs hepatic lipid homeostasis in livers of Creld2-deficient*
379 *mice*
380 Next, we turned to the question whether unresolved ER stress induces the observed
381 hepatosteatosis phenotype in *Creld2*$^{eGFP/eGFP}$ mice. To this end *Creld2*$^{eGFP/eGFP}$
382 animals and littermate controls received a single intraperitoneal injection of the ER
383 stressor Tm (1mg/kg), Tg (0.5 mg/kg) or sucrose as control and mice were analyzed
384 after two days (Figure 5A). Histological analyses as well as shotgun lipidomics
385 indicated that *Creld2*$^{WT/WT}$ livers did not accumulate lipids or glycogen after Tg
386 injection, while an increase of lipids and glycogen after Tm injection could be observed
387 (Figure 5B, C, S5A-C). The moderate lipid storage in *Creld2*$^{WT/WT}$ animals largely
388 resulted from accumulation of cholesterol and cholesterol esters (Figure 5C). Also
389 *Creld2*$^{eGFP/eGFP}$ animals did not present with increased lipid levels after Tg treatment
390 (Figure 5B, C, S5A-C). However, *Creld2*$^{eGFP/eGFP}$ livers stored more lipids than

391 *Creld2*$^{WT/WT}$ controls after Tm treatment, which could be mainly attributed to
392 augmented TAG, DAG and cholesterol ester abundance (Figure 5B, C). This fatty liver
393 phenotype was accompanied by a decreased PAS signal when compared to controls
394 (Figure 5B, S5C), similarly to the phenotype observed upon HFD-induced
395 hepatosteatosis. Further, MGT revealed an increased collagen storage after Tm
396 treatment in both genotypes (Figure S5D-E).

397 To identify the molecular mechanisms that lead to augmented lipid
398 accumulation in *Creld2*$^{eGFP/eGFP}$ mice after ER-stress induction with Tm and to
399 characterize the distinct tissue response after treatment with Tg, we performed RNA-
400 seq on livers and analyzed the gene expression using principle component analysis
401 (PCA, Figure S5F) and CoCena (Figure 5D, Table S7). The darkorange module (1257
402 genes) contains genes that were upregulated after Tm treatment in both genotypes
403 when compared to untreated mice, however, with even a higher expression in
404 *Creld2*$^{eGFP/eGFP}$ livers. KEGG pathway and GO enrichment returned terms such as
405 'NAFLD', 'glycoprotein metabolic process' and 'response to ER stress' (Figure 5D),
406 which comprised UPR- (*Atf6, Hspa5, Hsp90b1, Ern1*) and ERAD-related genes (*Derl1,*
407 *Derl3, Edem1, Pdia3, Pdia4, Sel1, Erlec1*) (Figure 5E). Tm treatment prevents protein
408 glycosylation, which in turn induces ER stress and lipid accumulation [15] (Figure 5B, C).
409 Wildtype livers largely recover from Tm-induced lipid perturbations after 2-3 days while
410 keeping part of the UPR active, e.g. expression of chaperones Grp78 and Grp94 [15,24].
411 Our data validate these observations showing that UPR is active after 2 days of Tm
412 treatment and further suggest that *Creld2*$^{eGFP/eGFP}$ livers undergo elevated ER stress
413 when compared to *Creld2*$^{WT/WT}$ controls. Yet, despite the increased UPR and ERAD
414 response on transcriptional level, *Creld2*$^{eGFP/eGFP}$ mice are unable to resolve ongoing
415 ER stress and thus present with increased hepatic lipid storage, supporting the active
416 role of Creld2 during UPR and subsequent ER protein processing capacity. In line with

417 this hypothesis, the module skyblue (273 genes) classified genes that are specifically
418 upregulated in *Creld2*$^{eGFP/eGFP}$ livers after Tm treatment (Figure 5D). GO enrichment
419 analysis of genes in the skyblue module included mainly terms related to 'mRNA
420 processing' as well as 'regulation of translational initiation', suggesting that *Creld2*-
421 deficient livers do not attenuate translation upon ER stress.

422 The module mediumorchide identified 298 genes that were globally
423 downregulated in *Creld2*$^{eGFP/eGFP}$ livers, with highest differences after Tm treatment
424 (Figure 5D). These genes enriched largely for 'lipid homeostasis' and 'glucose
425 metabolic process' as determined by GO enrichment analysis. Among enzymes
426 regulating metabolism homeostasis were *Dgat1*, *Dgat2*, *Abcd1*, *Acsm5*, *Cry2*, *Mup1*,
427 *Ormdl3,* and *Nr1h2* (lipid synthesis and storage) as well as *Adipor1* (glucose uptake)*,*
428 *Pklr, Shc1, Ppp1r3b,* and *Serpina12* (insulin response). The downregulation of hepatic
429 metabolism genes is in concordance with the phenotype observed in aged
430 *Creld2*$^{eGFP/eGFP}$ animals, arguing that accumulating ER stress in old Creld2-deficient
431 livers is responsible for these transcriptomic changes. Further, *Creld2*$^{eGFP/eGFP}$ livers
432 presented with a set of downregulated genes involved in biological processes of
433 protein catabolic processes (*Ppp1r15a*, *Grina, Creb3, Pdia2*, *Tmem259, Atg4b)*,
434 proteasome degradation (*Sqstm1, Rnf185, Rnf187, Fbxw5, Hectd3, Lrrc41, Ube3b,*
435 *Psmb5*) as well as (co)-chaperones (*Sgta, Hspbp1, Cdc37, Hspb6*), indicating that
436 catabolic processes induced upon ER stress to lower the protein load are attenuated
437 in a Creld2-dependent manner (Figure 5E).

438 Of note, the brown module contained 713 genes that were specifically
439 upregulated after Tg treatment in both genotypes and GO and Hallmark enrichment
440 analyses returned terms such as 'humoral immune response' and 'complement and
441 coagulation cascade', indicating that liver metabolism or the UPR is not affected by Tg
442 treatment. Taken together, our transcriptomic data show that *Creld2*$^{eGFP/eGFP}$ livers

443 efficiently induce the Atf6-dependent arm of the UPR and activate major components
444 of the ERAD machinery. Yet, the downregulation of genes within the E3-ubiquitin-
445 protein ligase complex and autophagosome suggests a dysfunctional UPR, which may
446 eventually result in increased protein accumulation due to inefficient protein
447 degradation.

448 To test this hypothesis, we first analyzed Grp78 protein abundance after Tg and
449 Tm treatment as an indicator for protein accumulation in the ER lumen. Similar to RNA-
450 seq results, Grp78 was upregulated in wildtype animals after Tm when compared to
451 control treatment, but was even more abundant in *Creld2*$^{eGFP/eGFP}$ livers (Figure 5F,
452 S5G). Of note, both GFP expression in *Creld2*$^{eGFP/eGFP}$ and Creld2 expression in
453 *Creld2*$^{WT/WT}$ littermate controls was increased upon both treatment conditions (Figure
454 5F, S5G), rendering Creld2 expression and the *Creld2*$^{WT/eGFP}$ mouse as an efficient
455 tool to monitor cellular stress. We next tested the activation of the Perk-axis via
456 analysis of Perk and eIF2a phosphorylation and Gadd34 protein abundance. Despite
457 the increased levels of Gpr78, we did not detect enhanced activation of the Perk-axis
458 in *Creld2*$^{eGFP/eGFP}$ livers (Figure 5F, S5G). In summary, induction of ER stress via Tm
459 partially recapitulates the phenotype observed in aged *Creld2*$^{eGFP/eGFP}$ animals
460 including increased Grp78 expression and hepatic lipid storage, supporting the notion
461 that Creld2 is required to maintain tissue homeostasis in order to prevent lipid
462 accumulation due to long-lasting and unresolved ER stress.

463

464 *Creld2 interaction partners*

465 To investigate the molecular function of Creld2 in UPR and metabolic homeostasis we
466 performed co-immunoprecipitation experiments by tandem affinity purification [27] and
467 subsequent mass spectrometry. We used mouse Creld2 tagged either on the N- or C-
468 terminus to exclude inhibition of protein binding due to the fused Strep-Flag tag.

469 Moreover, Creld2 constructs were either transiently expressed (72 h) or stably
470 integrated into the genome of HEK239 cells (Figure 6A) to *i)* enable the
471 characterization of specific interactions with chaperones since a strong transient
472 overexpression increases the unspecific co-purification of heat shock proteins [27] and
473 *ii)* select for highly conserved interactions, which would also occur in this inter-species
474 (mouse-human) setup. Using a stringed filtering pipeline and imputation (Figure 6B,
475 see also methods), we found 31 putative interaction partners (Figure 6C, Table S8).
476 Analysis for GO enrichment returned terms such as 'response to ER stress', 'protein
477 folding', and 'cell redox homeostasis' (Figure 6D). Many chaperones and protein
478 disulphide-isomerases (PDI) were present in the transient condition (C2-SF trans),
479 some of which (HSPA8, HSP90B, HYOU1) have been previously proposed to interact
480 with Creld2 [28]. However, since these proteins were not enriched in the stably
481 transfected cells (FS-C2 stab and C2-SF stab) we propose that these represent
482 unspecific co-purification products [27] underlining the constraints of co-
483 immunoprecipitation assays in transiently transfected cell lines.

484 We thus focused our analysis on candidates present in at least 2 conditions,
485 which contained CRELD2 itself, as expected, as well as HSPA5 (GRP78), thioredoxin
486 domain-containing 5 (TXNDC5) and glutathione S-transferase Mu3 (GSTM3) (Figure
487 6C). Interaction with GRP78 [28] confirms the active role of Creld2 in regulating UPR, as
488 it may sequester the chaperone away from Perk/Atf6/Ire1, thereby, promoting the
489 activation of the three UPR axes. TXNDC5, also known as endo PDI, is a thioredoxin
490 peroxidase whose expression is regulated by ATF6 and sXBP1. Functionally it is
491 proposed to reduce misfolded protein load [29]. Intriguingly, also Creld2 has been
492 proposed to have PDI-like functions [28], hinting towards a synergistic mechanism
493 between these proteins to resolve ER stress. GSTM3 is a member of the glutathione
494 S-transferases superfamily that promotes detoxification of reactive oxygen species

495 (ROS) [30]. Oxidative stress and UPR are tightly interlinked, exemplified by PERK being
496 upstream of the transcription factor NRF2 that counteracts the toxic effects of ROS
497 produced upon ER stress during protein folding, e.g. via PDI activity [31]. Thus, the
498 interaction of Creld2 with GSTM3 may represent an additional point of crosstalk
499 between these cellular stresses. In summary, our data strengthen the hypothesis of an
500 active involvement of Creld2 in UPR via interaction with chaperones and enzymes,
501 whose activity is required to overcome cellular stress.
502
503 CRELD2 expression in human liver disease
504 Overall, our data suggested that Creld2 function is required to maintain hepatic
505 homeostasis under physiological conditions during aging as well as during ER stress
506 responses in mice. Therefore, we next asked whether human CRELD2 would play a
507 role under pathophysiological conditions in the liver and analysed a cohort of 57 obese
508 patients with varying severity of non-alcoholic fatty liver disease (NAFLD) and 4
509 controls for CRELD2 expression. We first divided patients into two groups - with or
510 without NASH as diagnosed using the SAF (Steatosis, Activity and Fibrosis) score [32].
511 Intriguingly, both CRELD2 transcript and protein levels in the liver were significantly
512 upregulated in male patients with NASH, while expression in female patients remained
513 unaffected (Figure 7A). Control patients showed similar expression to NAFL patients.
514 To test whether secreted CRELD2 could be used as a diagnostic marker for NAFLD
515 severity we plotted the serum concentration of CRELD2 against the SAF score (Figure
516 7B). While no correlation was observed in female patients, males had an inverse
517 correlation with low levels of CRELD2 at higher SAF scores, which may hint towards
518 a retention mechanism for CRELD2 in the tissue during hepatic pathophysiology. In
519 summary, CRELD2 shows a sex-specific function during NAFLD in humans with an

520 intra-hepatic upregulation of CRELD2 expression, which seems to be associated with
521 progression to NASH in male patients.
522
523 **Discussion**
524 Our study shows that Creld2 plays an active role during UPR *in vitro* and *in vivo* and
525 contributes to the overall maintenance of cell homeostasis and resolution of ER stress
526 conditions. Using the newly generated *Creld2*$^{eGFP/eGFP}$ transgenic mouse model, we
527 characterized the stress response of *Creld2*-deficient cells. After challenge with Tm
528 and Tg, *Creld2*-deficient MEFs show perturbated induction of UPR, which ultimately
529 leads to their decreased survival. Dysregulation of UPR in *Creld2*-deficient MEFs is
530 evidenced by decreased or delayed induction of target genes and activation of proteins
531 within the Atf6 and Perk axes, including chaperones and ERAD machinery
532 components. Our *in vitro* data thus support the hypothesis that Creld2 is required to
533 protect cells against ongoing stress, although the cells retain the ability to partially
534 compensate through other signalling pathways.
535 Analysis of Creld2 interaction partners further strengthen its protective role
536 during the late phase of UPR: Creld2 protein accumulates 24-48h after induced ER
537 stress and has the capacity to bind to Grp78, which would in turn prohibit Grp78 from
538 binding to and inactivating Perk/Ire1/Atf6. Through this interaction, Creld2 may serve
539 as a positive feedback loop for UPR, thereby promoting continuous activity of the UPR
540 axes during long-lasting stress conditions. Further, Creld2 binds to the endo PDI
541 Txndc5 and glutathione S-transferase Gstm3, two proteins important for protein load
542 reduction and ROS detoxification, respectively. How binding to Creld2 influences the
543 function of these proteins remains to be investigated. Nevertheless, we propose that
544 Creld2 has a dual role during cellular stress: it keeps UPR elevated, most likely by
545 modulating the Perk- and Atf6-dependent axes through binding to Grp78, and at the

546 same time it contributes to the reduction of misfolded proteins either through its own
547 PDI activity or by promoting the PDI activity of Txndc5 and detoxification function of
548 Gstm3.

549 In line with our *in vitro* results, Creld2 function is a prerequisite *in vivo* particularly
550 in hepatocytes, a cell type that constantly undergoes increased levels of stress due to
551 its homeostatic function in the liver [33]. Albeit young animals can compensate for *Creld2*
552 deficiency, aged *Creld2*$^{eGFP/eGFP}$ animals present with a heightened UPR in the liver,
553 increased lipid accumulation, and disrupted glucose homeostasis. Since
554 *Creld2*$^{eGFP/eGFP}$ animals are generally not obese and show intact hepatic insulin
555 sensitivity, the long-lasting subthreshold UPR during ageing may indirectly contribute
556 to the observed systemic insulin resistance and glucose intolerance by promoting fat
557 accumulation in hepatocytes through the downregulation of lipid homeostasis
558 enzymes.

559 To test this hypothesis, we examined the line of causality between
560 hepatosteatosis and UPR by challenging young mice with Tm or Tg for 2 days or by
561 diet-induced obesity. We found no evidence that lipid accumulation through HFD *per*
562 *se* induces UPR in wildtype or *Creld2*$^{eGFP/eGFP}$ livers. Yet, livers from *Creld2*$^{eGFP/eGFP}$
563 animals show first signs of cellular stress and apoptosis when compared to controls,
564 which underlines the UPR-independent protective function of Creld2 upon oxidative
565 stress and ceramide-mediated hepatotoxicity caused by HFD [34,35]. Further, the diet
566 switch from HFD to CD did not promote ER-stress induction in both genotypes, but
567 rather reduced the expression of chaperones and induced genes important for lipid
568 homeostasis in *Creld2*$^{eGFP/eGFP}$ livers. Thus, we conclude that UPR does not play a
569 major role during diet-induced hepatic steatosis as long as this pathophysiology is
570 reversible and did not progress to NASH.

571 Despite a clear UPR induction in MEFs, our transcriptomic analysis in mice
572 confirmed that – in contrast to *in vitro* studies - *in vivo* treatment with Tg induced rather
573 hepatic inflammation and not ER stress [36]. Conversely, treatment with Tm led to
574 hepatic steatosis in *Creld2*$^{eGFP/eGFP}$ males mimicking the phenotype observed in aged
575 knockout animals. The increased hepatic lipid storage was accompanied by a
576 disrupted regulation of metabolic genes as well as a heightened ER stress and ERAD
577 response. However, despite enhanced UPR the tissue failed to induce proteasomal
578 catabolic processes indicating that *Creld2*$^{eGFP/eGFP}$ hepatocytes are unable to return to
579 homeostatic conditions. Thus, we conclude that *in vivo* Creld2 deletion sensitizes cells
580 to ER stress particularly in the liver, thereby, leading to long-lasting stress due to failure
581 of the protein folding and degradation machinery, which results in the observed tissue-
582 specific phenotype. The elevated stress response to Tm in the liver is in contrast to
583 what we observed *in vitro* where *Creld2*$^{eGFP/eGFP}$ MEFs failed to upregulate some
584 components of UPR signalling pathways upon Tg treatment. This could be due to the
585 time frame that cells experience Tg/Tm, to the distinct ER stressor, or may be
586 dependent on the cell type, underlined by the fact that Tg failed to induce hepatic ER
587 stress.

588 Similar to *Creld2*-deficient cells and mice, *Atf6*-knockout MEFs and animals
589 challenged with the ER stress-inducing agent Tm undergo persistent cell stress as they
590 are unable to upregulate ER chaperones and genes involved in ERAD. As a direct
591 consequence of this ongoing ER stress, metabolic genes are downregulated in the
592 liver [15]. Since Creld2 expression is regulated by Atf6 and *Creld2*$^{eGFP/eGFP}$ animals
593 suppress expression of genes maintaining lipid homeostasis even under unchallenged
594 conditions, we hypothesize that Atf6 restores overall cell homeostasis in a Creld2-
595 dependent manner. In this scenario Creld2 may be a candidate for a cross-talk

596 between the Atf6 and Perk pathway or between the UPR and protein folding machinery
597 (Figure 7C).

598 Intriguingly, we observed a sex dimorphism in aged mice, with only
599 *Creld2*$^{eGFP/eGFP}$ males presenting with steatosis while females were protected,
600 indicating that long-lasting unresolved ER stress induces hepatic pathophysiology
601 primarily in males. Sex differences in fatty liver diseases have been demonstrated both
602 in rodent models and in human disease [37]. NAFLD is more prevalent in men and
603 postmenopausal women compared to premenopausal women, which is mostly
604 attributed to hormone homeostasis and visceral fat accumulation [37,38]. However, we
605 did not observe general obesity or increased fat accumulation outside the liver in male
606 *Creld2*$^{eGFP/eGFP}$ mice. We therefore favor the hypothesis that the hepatic ER stress
607 response is sex dependent and thus a risk factor for the development of NAFLD and
608 progression to NASH or hepatocellular carcinoma (HCC) particularly in males. This is
609 in line with our results showing that CRELD2 accumulates only in livers of male NASH
610 patients, as well as a previous study demonstrating that kidneys of male mice are more
611 susceptible to ER stress-induced acute kidney injury than those of females due to a
612 testosterone-dependent mechanism [39]. Further, CRELD2 - among six other proteins
613 that maintain ER homeostasis - was identified as an adverse prognostic biomarker for
614 overall survival in HCC patients [40] underlining that elevated and unresolved ER stress
615 can promote liver pathophysiology. Therefore, it will be essential to take the sexual
616 dimorphism into account in the future when studying the contribution of ER stress to
617 hepatic steatosis as well as in the course of NAFLD treatment with UPR inhibitors.

618

619

620

621 **Materials and methods**

622 **Mouse work**

623 For the generation of a conventional *Creld2*$^{eGFP/eGFP}$ mouse the open reading frame
624 (ORF) of the *Creld2* gene was replaced by an enhanced green fluorescent protein
625 (eGFP) and a neomycin resistance cassette (neoR) flanked by two FRT sites via
626 homologous recombination. False positive ES cell clones were excluded by a
627 diphtheria toxin A (DTA) cassette, which was introduced after the 3' homologous region
628 of the targeting vector. Positive ES cell clones were selected by PCR against the neoR
629 cassette and confirmed by southern blot via an internal and 5' external probe.
630 Heterozygous Creld2$^{WT/eGFP/neo}$ offspring from blastocyst injections of positive ES cell
631 clones were crossed with mice ubiquitously expressing FLP recombinase for excision
632 of the neoR cassette. neoR deletion was confirmed by PCR. Mice were provided with
633 standard chow and autoclaved water ad libitum. Genotyping primers: Creld2 wt
634 genotype fw 5'-CCTGAGCTGTCCTTAGAAAGTTGCTAG-3', Creld2 ko genotype fw
635 5'-GCCCGACAACCACTACCTGAGC-3', Creld2 genotype rev 5'-
636 GGGGTTCATGTCCATGGGCCAC-3'.

637 For glucose tolerance test (GTT), mice were fasted for 6 h with supply of
638 drinking water ad libitum. Fasting blood glucose (0 min) was measured and mice were
639 injected with 2 g/kg glucose solution intraperitoneally (i.p.) and blood glucose was
640 measured after 15, 30, 60, 90, and 120 min. Blood samples were drawn from the tail
641 tip of the mice. Mice subjected to insulin tolerance test (ITT) had access to chow and
642 drinking water ad libitum before and throughout the experiment. Initial blood glucose
643 (0 min) was measured and mice were administered 0.75 U/kg insulin by i.p. injection
644 and blood glucose was measured as described for GTT.

645 To test hepatic insulin resistance, mice were fasted for 6 h with supply of
646 drinking water ad libitum prior to i.p. injection of glucose (2 g/kg). Mice were sacrificed
647 15 min after glucose administration and livers were harvested for further analysis.

648 To induce hepatic UPR, 8-9 weeks-old male mice were administered with Tg
649 (0.5 mg/kg), Tm (1 mg/kg) or a vehicle control sucrose solution (150 mM) via i.p.
650 injection and sacrificed after 48 h.

651 For HFD experiments, male mice received standard chow until 6 weeks of age.
652 Afterwards, standard chow was replaced by a control diet (CD; metabolizable energy:
653 62 % from carbohydrates, 11 % from fat, 27 % from protein; ssniff EF D12450B* mod.
654 LS) for 2 weeks prior to the beginning of the experiment. Subsequently, 8-week-old
655 mice were either fed with CD or HFD (metabolizable energy: 22 % from carbohydrates,
656 54 % from fat, 24 % from protein; ssniff EF acc. D12492 (I) mod.) for 12 weeks or mice
657 were kept on HFD for 8 weeks and CD for 4 weeks (HFD>CD). Mice were weighed
658 once a week. For the determination of the Homeostatic model assessment of insulin
659 resistance (HOMA-IR) [41], mice were fasted for 6 hours and blood was drawn from 8-
660 week-old mice at the beginning of the feeding period and from mice being fed CD or
661 HFD for 8 weeks. Blood samples were analyzed for blood glucose using a glucose
662 meter (Accu-Chek, Aviva) and blood serum insulin levels (Mouse Insulin Elisa kit,
663 Thermo Scientific) according to the manufacturers' instructions. HOMA-IR indices
664 were calculated using the formula: (Glucose (mg/ml) x Insulin(µU/ml))/405.

665 $$\frac{Glucose\ (mg^{ml-1}) \times Insulin\ (\mu U^{ml-1})}{405}$$

666 All mice were kept under standard SPF housing conditions according to the
667 approved animal license 84-02.04.2014.A335 with a 12 h dark/light cycle.

668

669

670

671 **Histological stainings**

672 For paraffin stains, tissues were fixed in 4% PFA (Thermo Scientific). After fixation,
673 tissues were dehydrated, paraffin embedded and cut at a thickness of 5 µm.
674 Subsequently, sections were deparaffinized, rehydrated and stained with Hematoxylin
675 followed by Eosin (VWR), PAS (Roth) or MGT (Merck) according to the manufacturer's
676 protocol. After dehydration, tissues were mounted in Entellan. For Cryo-embedded
677 (Tissue-Tek, Sakura) tissue stains, sections were fixed in 4% PFA and stained with
678 freshly prepared Oil-red-O (Sigma-Aldrich) working solution according to the
679 manufacturer's instructions followed by mounting in Kaiser's glycerol gelatine (Merck).
680 Quantitative analyses of PAS, MGT and ORO stainings were done using ImageJ2
681 software. Scripts for quantifications are provided at:
682 https://github.com/maccabaeus/histological-evaluation.git

683

684 **qPCR**

685 RNA was isolated using the Nucleospin RNA II kit (Macherey & Nagel) according to
686 the manufacturer's instructions and reverse transcribed into cDNA by using the
687 QantiTect reverse transcription kit (Qiagen) according to the manufacturer's
688 instructions. For qRT-PCR reactions, primer pairs (see Table S9 were mixed with
689 cDNA and iQ SYBR´Green Supermix (Bio-Rad), and qRT-PCR was run on an iQs
690 Real-Time PCR Detection System (Bio-Rad). Genes of interest were normalized to the
691 reference genes *Ppia* (peptidylprolyl isomerase A) and *Hprt* (hypoxanthine-guanine
692 phosphoribosyltransferase) for calculation of the Delta-Delta Cq value by the inherent
693 qRT-PCR evaluation software CFX manager (Bio-Rad). For human *CRELD2* gene
694 expression levels analysis *HPRT* was used as reference gene. Relative gene
695 expression was calculated from the threshold cycles in relation to the reference gene
696 and controls without NAFLD. Reactions were performed on a CFX96 Touch qPCR

697 System (Bio-Rad). To represent qRT-PCR as heatmaps, gene expression data
698 (housekeeper normalized delta delta Cq values) were scaled to individual genes
699 separately for each gender prior to averaging and plotting of heatmaps using the
700 pheatmap R-package.
701
702 **Bone marrow-derived macrophage (BMDM) isolation and LSP treatment**
703 Femur and tibia of sacrificed mice were dissected and flushed with PBS using a 26G
704 needle and cultured in DMEM (Invitrogen) medium supplied with 10% FCS (Pan
705 Biotech), 1% Pen-Strep (10000 U/mL; Thermo Scientific), 20% L929 cell medium
706 supernatant for 6 days. Subsequently, differentiated BMDMs were stimulated with LPS
707 (200 ng/ml; from *Escherichia coli* O111:B4; Sigma-Aldrich) for 4-8 h.
708
709 **Kupffer cells flow cytometry**
710 Livers were harvested and incubated in digestion buffer (PBS, 1 mg/ml collagenase D
711 (Roche), 100 U /ml DNase I (Sigma-Aldrich), 2.4 mg/ml dispase (Invitrogen), 3% FCS
712 (Invitrogen)) at 37°C for 30 min prior to mechanical disruption by straining through a
713 100 µm cell filter. Cell suspensions were centrifuged at 50 g for 3 min to sediment
714 hepatocytes, supernatants were recovered, centrifuged at 320 g for 7 min and
715 incubated in FACS buffer (PBS, 0.5% BSA, 2 mm EDTA) containing anti-CD16/32
716 (1:100 dilution), 5% normal mouse, 5% normal rabbit and 5% normal rat serum for 15
717 min at 4°C. After the incubation, cells were immunostained with antibody mixtures
718 (CD45-APC/Cy7 (30-F100), CD11b-PECy7 (M1/70), F4/80-BV421 (BM8), Tim4-
719 AF647 (RMT4-54) (all from Biolegend)) for 30 min at 4°C. Single live cells were
720 selected by excluding dead cells (Hoechst 33258, 1:10.000), gating on side (SSC-A)
721 and forward scatter (FSC-A) and excluding doublets using forward scatter width (FSC-

722 W) against FSC-A. Kupffer cells were identified by gating on $CD45^+$, $CD11b^{low}$,
723 $F4/80^+Tim4^+$ cells.
724
725 **Cell culture**
726 Pregnant mice were sacrificed and embryos (E12.5) were obtained. Heart and liver of
727 embryos were removed and embryo bodies were incubated in trypsin-EDTA (Thermo
728 Scientific) for 30 min at 37°C with shaking at 900 rpm. After digestion, cells were
729 centrifuged at 100 g for 5 min, washed once with DMEM and cultured in DMEM at
730 37°C. Experiments were conducted on cells at passage 4. For acute ER stress
731 induction $0.5x10^6$ MEF cells were treated with 1 µM Tg for 1-8 h and either harvested
732 for further analysis, or split and $1x10^4$ cells were seeded out in a 24-well plate and
733 cultured for another 5 days in DMEM without Tg for cell viability analysis. For recovery
734 experiments, MEFs were treated with 1 µM Tg for 2 h and further cultured without ER
735 stressor for up to 46 h. For induction of chronic ER stress, cells were treated with Tg
736 (2.5, 5, 10 nM, Sigma-Aldrich) for up to 48 h or Tm (25, 50,100 ng/ml, Sigma-Aldrich)
737 for up to 72 h. Control cells (0 h) were cultured in DMEM supplied with DMSO mock.
738 For crystal violet survival assays, MEFs were fixed with Histofix 4% (Roth) for 5 min,
739 stained with Crystal violet (0.05% in ddH_2O; Roth) for 30 min followed by washing twice
740 with tap water and subsequent air-drying. After drying, dye was solubilized by addition
741 of MeOH and staining intensity was measured photometrically at 590 nm (Fluostar
742 Omega; BMG Labtech).
743
744 **Library preparation for RNA sequencing**
745 mRNA was converted into libraries of double stranded cDNA molecules as a template
746 for high throughput sequencing following the SMART-Seq2 protocol [42]. Shortly, mRNA
747 was primed for SMART reverse transcription from 5 ng of total RNA using poly-T oligos.

748 cDNA was pre-amplified by SMART ISPCR. Fragmentation was performed using the
749 Illumina Nextera XT kit, followed by PCR amplification and indexing. Size-selection
750 and purification of library fragments with preferentially 300-400 bp in length was
751 performed using SPRIBeads (Beckman-Coulter). The size-distribution of cDNA
752 libraries was measured using the Agilent high sensitivity D5000 assay on a Tapestation
753 4200 system (Agilent). cDNA libraries were quantified using a Qubit high sensitivity
754 dsDNA assay. 75 bp single-end sequencing was performed on a NextSeq500 system
755 using High Output v2.5 chemistry. Base calling from base call files, alignment to the
756 Mus musculus reference genome mm10 from UCSC and file conversion to fastq files
757 were achieved by Illumina standard pipeline scripts (STAR version, bcl2fastq2 v.2.20).
758

759 **RNA sequencing analysis**

760 Kallisto [43] was used to quantify abundances of transcripts - read counts - from the bulk
761 RNA-seq data. The kallisto read counts were used as input to DESeq2 [44] for calculation
762 of normalized signal signal and differentially gene expression analysis. Genes are
763 excluded from the analysis where the total read count of all samples is less than 10.
764 This pre-filtering step removes genes in which there are very few reads, in order to
765 reduce the memory size, and to increase the speed of the calculation. The diet and
766 drug induced ER-stress dataset then comprised 17340 and 17280 genes respectively.
767 DESeq Dataset (dds) was created to store the read counts and the intermediate
768 estimated quantities with a merged design formula consist of genotype (*Creld2*$^{WT/WT}$ or
769 *Creld2*$^{eGFP/eGFP}$) and condition (dietary or pharmacological). The quality control of the
770 samples shows the variance of the read counts between the samples, where dds was
771 used as an input file. Variance stabilizing transformations (VST) were used for the
772 downstream analysis (clustering). VST produces transformed data on the log2 scale
773 which has been normalized with respect to library size. Date of experiment was

774 modelled as a known batch factor using the "Linear Models for Microarray and RNA-
775 Seq Data" (Limma) package [45]. Unwanted surrogate variables were estimated and
776 modelled via Surrogate Variable Analysis (SVA) [46] using the method called leek. In the
777 diet related experiment 22 surrogate variables (SV) were identified and 3 of them
778 modelled. The top 5000 variable genes were selected and used as an input for co-
779 expressional network analysis using CoCena2
780 (https://github.com/UlasThomas/CoCena2). Person correlation analysis was performed
781 with correlational significance measure $p<0.05$. For the diet-induced dataset 0.712
782 and for the pharmacologically-induced dataset 0.791 was identified as correlation
783 coefficient cut-off. Based on a greedy approach, Louvain community detecting
784 algorithm [47] was used to cluster the genes based on expression pattern between the
785 different conditions. Clustering was repeated 100 times. Minimal number of genes per
786 cluster was set to 50. Gene set enrichment analysis (GSEA) was performed on all
787 gene-clusters using the following knowledge-bases: Hallmark, Reactome, GO, KEGG
788 and DO. ClusterProfiler package [48] was used for all GSEAs using default options. The
789 prior mechanisms associated with the Co-Cena clusters were manually selected from
790 the GSEA results based on prior knowledge.
791

792 **Thin layer chromatography**

793 Total lipids were extracted as described by Bligh and Dyer [49]. Livers were
794 homogenized in ice cold H_2O (50mg wet weight/ml) in a Precellys homogenizer
795 (Peqlab Biotechnology, Germany). 3 ml of chloroform/methanol 1:2 (v:v) were added
796 to 800 µl homogenate and vortexed. 1 ml of chloroform was added to the mixture and
797 vortexed prior to addition of 1 ml H_2O and thoroughly vortexed. Mixture was centrifuged
798 at 1000 g for 5 min at RT and the lower solvent phase was recovered. Same volumes
799 of the solvent phase were evaporated under nitrogen and lipids were resuspended in

800 100 µl of chlorophorm/methanol 1:1 (v:v) (Merck). Lipid extracts corresponding to 1 mg
801 wet liver weight were applied onto HPTLC silica gel 60 plates (10 X 20 cm: Merck) and
802 plates were developed in *n*-hexane/diethylether/acetic acid 70:30:5 (v/v/v) (Merck,
803 Roth) in a developing chamber (CAMAG, Switzerland). Dried plates were soaked in
804 charring solution (copper sulfate ($CuSO_4$) 10% and phosphoric acid (H_2PO_4) 8%
805 (Roth)) and heated to 180 °C for 5-10 min for lipid visualization.
806

807 **Lipid mass spectrometry**

808 Livers were homogenized in ddH_2O at a concentration of 20 mg (wet weight)/ml using
809 a Precellys homogenizer (Peqlab Biotechnolog, Germany). For lipid extraction, 50 µl
810 of the homogenate were added to 500 µl of extraction mix ($CHCl_3$/MeOH 1/5 containing
811 internal standards: 210 pmol PE(31:1), 396 pmol PC(31:1), 98 pmol PS(31:1), 84 pmol
812 PI(34:0) , 56 pmol PA(31:1), 51 pmol PG (28:0), 28 pmol CL(56:0), 39 pmol LPA (17:0),
813 35 pmol LPC(17:1), 38 pmol LPE (17:0), 32 pmol Cer(17:0), 99 pmol SM(17:0), 55
814 pmol GlcCer(12:0), 14 pmol GM3 (18:0-D3), 359 pmol TG(47:1), 111 pmol CE(17:1),
815 64 pmol DG(31:1), 103 pmol MG(17:1), 724 pmol Chol(d6), 45 pmol Car(15:0)) were
816 added and the sample sonicated for 2 min followed by centrifugation at 20000 g for 2
817 min. The supernatant was collected into a new tube and 200 µl chloroform and 800 µl
818 1% AcOH in water were added, the sample briefly shaken and centrifuged for 2 min at
819 20000 g. The upper aqueous phase was removed and the entire lower phase
820 transferred into a new tube and evaporated in the speed vac (45°C, 10 min). Spray
821 buffer (500 µl of 8/5/1 2-propanol/MeOH/water, 10 mM ammonium acetate) was
822 added, the sample sonicated for 5 min and infused at 10 µl/min into a Thermo Q
823 Exactive Plus spectrometer equipped with the HESI II ion source for shotgun
824 lipidomics. MS1 spectra (resolution 280000) were recorded in 100 m/z windows from
825 250 – 1200 m/z (pos.) and 200 – 1700 m/z (neg.) followed by recording MS/MS spectra

826 (res. 70000) by data independent acquisition in 1 m/z windows from 200 – 1200 (pos.)
827 and 200 – 1700 (neg.) m/z. Raw files were converted to .mzml files and imported into
828 and analysed by LipidXplorer software using custom mfql files to identify sample lipids
829 and internal standards. For further data processing, absolute amounts were calculated
830 using the internal standard intensities followed by calculation of mol% of the identified
831 lipids.
832
833 **Tandem affinity purification of tagged Creld2**
834 HEK293 cells were electroporated with plasmid DNA pcDNA3.1/Zeo(+) (Addgene)
835 containing only the Strep-Flag (SF)-tag (mock), N-terminally tagged Creld2 (FS-C2)
836 where the tag was integrated after the signal peptide or C-terminally tagged Creld2
837 (C2-SF). Gene blocks were used to clone the constructs (see Table S10). Primer used
838 for cloning:
839 NheI-Kozak-mC2-SF-tag fw 5‘-CTAGCTAGCGCCACCATGCACCTGCTGCTTGCA-
840 3’, 5’-Creld2-KpnI TATGGTACCTCACAAATCCTCACGGGAGGG-3’,
841 KpnI-Flag rev 5’-TAGGGTACCTCACTTGTCGTCGTC-3’,
842 NheI-SF-tag fw 5’-CTAGCTAGCATGGGTGGAGGTTCTGGA-3’,
843 KpnI-SF-tag rev 5’-GGAGCTCTGGATGGTACCTCACTTGTC-3’.
844 Plasmids comprised a zeocin resistance cassette for selection. Cells transiently
845 expressing C2-SF were harvested 72 h post electroporation for tandem-affinity-
846 purification (TAP). For the generation of stably expressing cell lines plasmid DNA was
847 linearized prior to electroporation and selected for stable expression by Zeocin (200
848 µg/ml) resistance for 4 weeks with validation of construct expression via
849 immunoblotting against Creld2 and Flag. For TAP cells were incubated on ice in freshly
850 prepared, ice cold TAP-lysis buffer (1x Complete protease inhibitor (Roche), 1x
851 Phosphate inhibitor cocktail (PIC) I (Sigma-Aldrich), 1x PIC II (Sigma-Aldrich), 0.5%

852 NP40 in 1x TBS) for 20 min, centrifuged for 10 min at 10000 g at 4°C and supernatant
853 was recovered. Subsequently, lysates were incubated with Strep-tactin Sepharose
854 resin (IBA) for 2 h at 4°C on a rotation wheel. After incubation lysates were transferred
855 onto Micro Bio-Spin columns (0.8 ml, BioRad), washed 3 times with TAP-wash buffer
856 (1x PIC I, 1x PIC II, 0.1% NP40 in 1x TBS) and incubated with TAP-elution buffer (50
857 µM Desthiobiotin (IBA) in 1x TBS) at 4°C for 10 min prior to elution by centrifugation at
858 100 g for 10 sec. Eluates were incubated with anti-Flag M2 resin (Sigma-Aldrich) for 2
859 h at 4°C on a rotation wheel, washed once with TAP-wash buffer, twice with TBS and
860 eluted by incubating samples with Flag elution buffer (200 µg/ml Flag peptide (Sigma-
861 Aldrich) in 1x TBS) for 10 min following centrifugation for 10 sec at 2000 g. TAPs were
862 performed in triplicates from cells harvested on different days.
863
864 Processing of TAP proteins for mass spectrometry and analysis:
865 Eluates were reduced with 10 mM Dithiothreitol (DTT) for 30 min at 56 °C followed by
866 alkylation with 55 mM Chloroacetamide (CAA) for 30 min at RT in the dark.
867 Subsequently, samples were boiled in laemmli buffer (1 x final concentration 2% SDS,
868 2 µM DTT, 5% (v/v) Glycerol, 50 µM Tris-HCL (pH 6.8, 0.01% (w/v) Bromophenol blue)
869 at 95 °C for 10 min and run for approx. 1 cm in a 10% SDS-PAGE gel to separate
870 purified proteins from the Flag peptide used for elution. Gels were fixed in fixation buffer
871 (45 % H_2O, 45 % MeOH, 10 % Acetic acid) for 1 h at RT and stained (fixation buffer,
872 0.05 % Coomassie-G250, filtered) for 1 h at RT followed by a first destaining in fixation
873 buffer for 1 h prior to destaining O/N. Protein lanes were separated, cut into small
874 pieces, washed twice with MS-wash buffer (50 mM Ammonium bicarbonate (ABC), 50
875 % Acetonitrile (ACN)) for 20 min, dehydrated with ACN for 10 min and dried in a speed
876 vac for 20 min. Afterwards, samples were washed with 50 mM ABC for 15 min at RT
877 and dehydration was repeated with speed vacuuming for 30 min. For in-gel-digest of

878 proteins, gel pieces were soaked in digest solution (0,009 µg/µl Trypsin, 0,001 µg/µl
879 LysC, 45 mM ABC) for 30 min at 4 °C, covered with 50 mM ABC and digested O/N at
880 37 °C. Supernatants were recovered, gel pieces incubated in extraction buffer (30 %
881 ACN, 3 % Trifluoroacetic acid (TFA)) for 20 min at RT, supernatants were recovered
882 and proteins were extracted for another time from gel pieces by incubation in 100 %
883 ACN for 20 min at RT with recovery of supernatants. The recovered supernatants of
884 individual samples were pooled, organic solvents were evaporated in a speed vac,
885 samples were acidified with Formic acid (1 % final concentration), stage tipped and
886 subjected to mass spectrometry.
887
888 TAP mass spectrometry
889 Raw mass spectrometry data files were analyzed using MaxQuant software (version
890 1.6.0.16). Further analysis of quantitated proteins was done with Perseus software
891 (version 1.5.5.3). Data was cleaned by filtering out of reverse proteins, proteins only
892 identified by site and contaminants, and filtered for valid proteins label-free
893 quantification (LFQ) values identified in at least 2 technical replicates in minimum 1
894 condition. Further analysis of data was done using R software. Missing LFQ values
895 were imputed using the DEP package by firstly imputing of missing not at random
896 (MNAR) values with 0, followed by a screen for falsely categorized MNAR values and
897 re-imputation of missing at random (MAR) values using the k-nearest neighbor (knn)
898 algorithm. For statistical analysis of differentially enriched (DE) proteins two-tailed t-
899 test with unequal variance was applied to conditions containing Creld2 protein versus
900 the respective mock control (acute or stable). Proteins with fold change > 0 (Creld2
901 containing conditions versus mock control) and p-value < 0.1 were considered
902 differentially enriched.
903

904

905 **Patients and ethics**

906 The study protocol conformed to the revised Declaration of Helsinki (Edinburgh, 2000)
907 and was approved by the local Institutional Review Board (Ethik-Kommission am
908 Universitätsklinikum Essen; file number 09-4252). All patients provided written
909 informed consent for participation in the study before recruitment. Liver tissue and
910 serum were collected from morbidly obese patients undergoing bariatric surgery. All
911 enrolled patients underwent physical and ultrasound examinations, and a complete set
912 of laboratory studies. Subjects reporting excessive alcohol consumption (>20 g/day for
913 men or >10 g/day for women) and those with other known causes of secondary fatty
914 liver disease (e.g., viral hepatitis, metabolic liver disease, toxic liver disease) were
915 excluded from the study. Histological evaluation of NAFLD and classification as NAFL
916 or NASH were performed by two experienced pathologists according to the method of
917 Bedossa et al. (SAF score [32]).

918

919 **CRELD2 ELISA**

920 Serum CRELD2 levels were measured using a human CRELD2 Elisa kit (Ray Biotech)
921 according to the manufacturers' instructions.

922

923 **Immunoblotting**

924 Human tissue samples: Liver tissue was directly lysed for 30 min on ice with RIPA
925 Lysis and Extraction Buffer (Thermo Scientific) containing protease inhibitor cocktail
926 and phosphostop (Roche). After centrifugation at 13 000 g for 15 min at 4 °C, protein
927 concentration in the supernatant was measured using Bradford's reagent (Bio-Rad).
928 Mouse tissue samples: Tissue was snap frozen in liquid N_2 and stored at -80 °C until
929 usage. Tissue was homogenized in RIPA buffer containing PIC I and PIC II (Sigma-

930 Aldrich) and Complete protease inhibitor (Roche) using a Precellys homogenizer and
931 lysed for 30 min on ice. 10-20 µg of total protein were separated by SDS-PAGE and
932 transferred onto a PVDF membrane (Immobilon-P transfer membranes 0.45 µm,
933 Merck) via semi-dry blotting (Trans-Blot Turbo Transfer System, Bio-Rad). If not
934 otherwise mentioned, membranes were incubated with antibodies diluted in TBST
935 (0.1% Tween20) over night at 4°C on a rocker with the particular antibodies (see Table
936 S11). Protein band intensities were acquired using ImageJ2. Proteins of one
937 membrane were normalized to Actin and set relative to a wildtype control located on
938 the membrane.

939

940 **Statistical analysis and reproducibility**

941 Data are shown as mean with individual values per mouse represented as circles,
942 unless stated otherwise. Statistical significance was analysed with R using unpaired
943 two-tailed t-tests, one-way and two-way ANOVA as indicated in the figure legends. The
944 n value represents biological replicates. Significance was considered at $P < 0.05$.
945 Experiments were repeated to ensure reproducibility of the observations. Equal
946 variance was assumed for cell-counting experiments. No statistical methods were used
947 to predetermine sample size.

948

949 **Data availability**

950 Gene expression data are currently being deposited in the GEO database. Lipid mass
951 spectrometry data are deposited in a Github repository
952 https://github.com/maccabaeus/Creld2-lipid-mass-spectrometry.git). The data that
953 support the findings of this study are available from the corresponding author upon
954 reasonable request.

955

Acknowledgements

We thank Prof. Michael Hoch for his long-standing support of this project. We thank Thomas D. Rutkowski for feedback on the manuscript. We thank Cornelia Cygon and Melanie Thielisch for technical support, and Dr. Joachim Degen for help with the generation of *Creld2*$^{eGFP/eGFP}$ mice. We would like to thank Prof. Margarete Odenthal (Institute for Pathology, University Hospital Cologne), Prof. Hideo A. Baba und Martin Schlattjan (Institute for Pathology, University Hospital Essen), and Prof. Johannes Haybäck (Institute for Pathology, University Hospital Magdeburg) for histological preparation and assessments for the validation cohort. We also thank Prof. Niedergethmann (Department for General- and Visceral Surgery, Alfried Krupp Hospital, Essen, Germany) and Prof. Hasenberg (Helios Hospital Niederberg) for sample collection of the validation cohort. AC was funded by the DFG CA267/14-1. EM and JLS were funded by the DFG under Germany's Excellence Strategy EXC2151-390873048. EM is supported by the Daimler and Benz Foundation. This work was funded by the Fritz Thyssen foundation (to EM, Az.10.18.2.029MN).

Competing interests

The authors declare no competing interests

Contributions

EM and PK conceived the project. PK, EM, AF, LB, FB performed experiments. PK, EM, NB, AF analyzed data. EM, PK, and RB supervised experiments and data analysis. TU and JLS provided help with RNA-seq experiments and the script for CoCena analyses. CT helped with lipidomic analyses. JPS and AC assisted in interpretation of human results. EM and PK wrote the manuscript.

982 **References**

983 1. Rupp, P. A. *et al.* Identification, genomic organization and mRNA expression of
984 CRELD1, the founding member of a unique family of matricellular proteins.
985 *Gene* **293**, 47–57 (2002).
986 2. D'Alessandro, M. *et al.* CRELD1 is an evolutionarily-conserved maturational
987 enhancer of ionotropic acetylcholine receptors. *Elife* **7**, (2018).
988 3. Oh-hashi, K., Kunieda, R., Hirata, Y. & Kiuchi, K. Biosynthesis and secretion of
989 mouse cysteine-rich with EGF-like domains 2. *FEBS Lett.* **585**, 2481–2487
990 (2011).
991 4. Mass, E., Wachten, D., Aschenbrenner, A. C., Voelzmann, A. & Hoch, M.
992 Murine Creld1 controls cardiac development through activation of
993 calcineurin/NFATc1 signaling. *Dev. Cell* **28**, (2014).
994 5. Kim, Y. *et al.* Elevated urinary CRELD2 is associated with endoplasmic
995 reticulum stress–mediated kidney disease. *JCI Insight* **2**, (2017).
996 6. Chen, M.-F. *et al.* Synovial fluid interleukin-16, interleukin-18, and CRELD2 as
997 novel biomarkers of prosthetic joint infections. *Bone Joint Res.* **8**, 179–188
998 (2019).
999 7. Oh-hashi, K. *et al.* CRELD2 is a novel endoplasmic reticulum stress-inducible
1000 gene. *Biochem. Biophys. Res. Commun.* **387**, 504–510 (2009).
1001 8. Oh-hashi, K. *et al.* Role of an ER stress response element in regulating the
1002 bidirectional promoter of the mouse CRELD2 - ALG12 gene pair. *BMC*
1003 *Genomics* **11**, 664 (2010).
1004 9. Walter, P. & Ron, D. The Unfolded Protein Response: From Stress Pathway to
1005 Homeostatic Regulation. *Science (80-.).* **334**, 1081–1086 (2011).
1006 10. Song, M. J. & Malhi, H. The unfolded protein response and hepatic lipid
1007 metabolism in non alcoholic fatty liver disease. *Pharmacol. Ther.* 107401

1008 (2019). doi:10.1016/j.pharmthera.2019.107401
1009 11. Fu, S. *et al.* Aberrant lipid metabolism disrupts calcium homeostasis causing
1010 liver endoplasmic reticulum stress in obesity. *Nature* **473**, 528–31 (2011).
1011 12. Ozcan, U. *et al.* Endoplasmic Reticulum Stress Links Obesity, Insulin Action,
1012 and Type 2 Diabetes. *Science (80-.).* **306**, 457–461 (2004).
1013 13. Ozcan, U. *et al.* Chemical chaperones reduce ER stress and restore glucose
1014 homeostasis in a mouse model of type 2 diabetes. *Science* **313**, 1137–40
1015 (2006).
1016 14. Kammoun, H. L. *et al.* GRP78 expression inhibits insulin and ER stress-
1017 induced SREBP-1c activation and reduces hepatic steatosis in mice. *J. Clin.*
1018 *Invest.* **119**, 1201–15 (2009).
1019 15. Rutkowski, D. T. *et al.* UPR Pathways Combine to Prevent Hepatic Steatosis
1020 Caused by ER Stress-Mediated Suppression of Transcriptional Master
1021 Regulators. *Dev. Cell* **15**, 829–840 (2008).
1022 16. Yamamoto, K. *et al.* Induction of liver steatosis and lipid droplet formation in
1023 ATF6alpha-knockout mice burdened with pharmacological endoplasmic
1024 reticulum stress. *Mol. Biol. Cell* **21**, 2975–86 (2010).
1025 17. DeZwaan-McCabe, D. *et al.* ER Stress Inhibits Liver Fatty Acid Oxidation while
1026 Unmitigated Stress Leads to Anorexia-Induced Lipolysis and Both Liver and
1027 Kidney Steatosis. *Cell Rep.* **19**, 1794–1806 (2017).
1028 18. Oh-Hashi, K., Fujimura, K., Norisada, J. & Hirata, Y. Expression analysis and
1029 functional characterization of the mouse cysteine-rich with EGF-like domains 2.
1030 *Sci. Rep.* **8**, 12236 (2018).
1031 19. Soontornniyomkij, V. *et al.* Age and High-Fat Diet Effects on Glutamine
1032 Synthetase Immunoreactivity in Liver and Hippocampus and Recognition
1033 Memory in Mice. *Curr. Aging Sci.* **9**, 301–309 (2016).

1034 20. Birkenfeld, A. L. & Shulman, G. I. Nonalcoholic fatty liver disease, hepatic
1035 insulin resistance, and type 2 diabetes. *Hepatology* **59**, 713–23 (2014).
1036 21. Gruben, N., Shiri-Sverdlov, R., Koonen, D. P. Y. & Hofker, M. H. Nonalcoholic
1037 fatty liver disease: A main driver of insulin resistance or a dangerous liaison?
1038 *Biochim. Biophys. Acta - Mol. Basis Dis.* **1842**, 2329–2343 (2014).
1039 22. Adachi, Y. *et al.* ATF6 Is a Transcription Factor Specializing in the Regulation
1040 of Quality Control Proteins in the Endoplasmic Reticulum. *Cell Struct. Funct.*
1041 **33**, 75–89 (2008).
1042 23. Lefere, S. & Tacke, F. Macrophages in obesity and non-alcoholic fatty liver
1043 disease: Crosstalk with metabolism. *JHEP Reports* **1**, 30–43 (2019).
1044 24. Wu, J. *et al.* ATF6alpha optimizes long-term endoplasmic reticulum function to
1045 protect cells from chronic stress. *Dev. Cell* **13**, 351–64 (2007).
1046 25. Kuipers, E. J. *et al.* REVIEWS IN BASIC AND CLINICAL
1047 GASTROENTEROLOGY AND HEPATOLOGY Bioactive Lipid Species and
1048 Metabolic Pathways in Progression and Resolution of Nonalcoholic
1049 Steatohepatitis. (2018). doi:10.1053/j.gastro.2018.06.031
1050 26. Musso, G., Cassader, M., Paschetta, E. & Gambino, R. Bioactive Lipid Species
1051 and Metabolic Pathways in Progression and Resolution of Nonalcoholic
1052 Steatohepatitis. *Gastroenterology* **155**, 282-302.e8 (2018).
1053 27. Gloeckner, C. J., Boldt, K., Schumacher, A. & Ueffing, M. Tandem affinity
1054 purification of protein complexes from mammalian cells by the Strep/FLAG
1055 (SF)-TAP tag. *Methods Mol. Biol.* **564**, 359–72 (2009).
1056 28. Hartley, C. L. *et al.* Armet/Manf and Creld2 are components of a specialized
1057 ER stress response provoked by inappropriate formation of disulphide bonds:
1058 implications for genetic skeletal diseases. *Hum. Mol. Genet.* **22**, 5262–75
1059 (2013).

1060 29. Horna-Terrón, E., Pradilla-Dieste, A., Sánchez-de-Diego, C. & Osada, J.
1061 TXNDC5, a newly discovered disulfide isomerase with a key role in cell
1062 physiology and pathology. *Int. J. Mol. Sci.* **15**, 23501–18 (2014).
1063 30. Board, P. G. & Menon, D. Glutathione transferases, regulators of cellular
1064 metabolism and physiology. *Biochim. Biophys. Acta - Gen. Subj.* **1830**, 3267–
1065 3288 (2013).
1066 31. Zhang, Z. *et al.* Redox signaling and unfolded protein response coordinate cell
1067 fate decisions under ER stress. *Redox Biol.* (2018).
1068 doi:10.1016/J.REDOX.2018.11.005
1069 32. Bedossa, P. *et al.* Histopathological algorithm and scoring system for
1070 evaluation of liver lesions in morbidly obese patients. *Hepatology* **56**, 1751–
1071 1759 (2012).
1072 33. Han, J. & Kaufman, R. J. The role of ER stress in lipid metabolism and
1073 lipotoxicity. *Journal of Lipid Research* **57**, 1329–1338 (2016).
1074 34. Longato, L., Tong, M., Wands, J. R. & de la Monte, S. M. High fat diet induced
1075 hepatic steatosis and insulin resistance: Role of dysregulated ceramide
1076 metabolism. *Hepatol. Res.* **42**, 412–27 (2012).
1077 35. Kurek, K. *et al.* Inhibition of ceramide de novo synthesis reduces liver lipid
1078 accumulation in rats with nonalcoholic fatty liver disease. *Liver Int.* **34**, 1074–
1079 1083 (2014).
1080 36. Abdullahi, A., Stanojcic, M., Parousis, A., Patsouris, D. & Jeschke, M. G.
1081 Modeling Acute ER Stress in Vivo and in Vitro. *SHOCK* **47**, 506–513 (2017).
1082 37. Ballestri, S. *et al.* NAFLD as a Sexual Dimorphic Disease: Role of Gender and
1083 Reproductive Status in the Development and Progression of Nonalcoholic Fatty
1084 Liver Disease and Inherent Cardiovascular Risk. *Advances in Therapy* **34**,
1085 1291–1326 (2017).

1086 38. Lonardo, A. & Suzuki, A. Nonalcoholic fatty liver disease: does sex matter?
1087 *HepatoBiliary Surg. Nutr.* **8**, 164–166 (2019).
1088 39. Hodeify, R. *et al.* Gender differences control the susceptibility to ER stress-
1089 induced acute kidney injury. *Am. J. Physiol. - Ren. Physiol.* **304**, (2013).
1090 40. Liu, G.-M., Zeng, H.-D., Zhang, C.-Y. & Xu, J.-W. Key genes associated with
1091 diabetes mellitus and hepatocellular carcinoma. *Pathol. - Res. Pract.* 152510
1092 (2019). doi:10.1016/j.prp.2019.152510
1093 41. Matthews, D. R. *et al.* Homeostasis model assessment: insulin resistance and
1094 beta-cell function from fasting plasma glucose and insulin concentrations in
1095 man. *Diabetologia* **28**, 412–9 (1985).
1096 42. Picelli, S. *et al.* Smart-seq2 for sensitive full-length transcriptome profiling in
1097 single cells. *Nat Methods* **10**, 1096–1098 (2013).
1098 43. Bray, N. L., Pimentel, H., Melsted, P. & Pachter, L. Near-optimal probabilistic
1099 RNA-seq quantification. *Nat. Biotechnol.* **34**, 525–527 (2016).
1100 44. Love, M. I., Huber, W. & Anders, S. Moderated estimation of fold change and
1101 dispersion for RNA-seq data with DESeq2. *Genome Biol* **15**, 550 (2014).
1102 45. Ritchie, M. E. *et al.* Limma powers differential expression analyses for RNA-
1103 sequencing and microarray studies. *Nucleic Acids Res.* **43**, e47 (2015).
1104 46. Leek, J. *et al.* sva: Surrogate Variable Analysis. R package version 3.34.0.
1105 (2019).
1106 47. Blondel, V. D., Guillaume, J. L., Lambiotte, R. & Lefebvre, E. Fast unfolding of
1107 communities in large networks. *J. Stat. Mech. Theory Exp.* **2008**, (2008).
1108 48. Yu, G., Wang, L. G., Han, Y. & He, Q. Y. clusterProfiler: an R package for
1109 comparing biological themes among gene clusters. *OMICS* **16**, 284–287
1110 (2012).
1111 49. BLIGH, E. G. & DYER, W. J. A rapid method of total lipid extraction and

1112 purification. *Can. J. Biochem. Physiol.* **37**, 911–917 (1959).

1113

Kern et al. Fig. 1

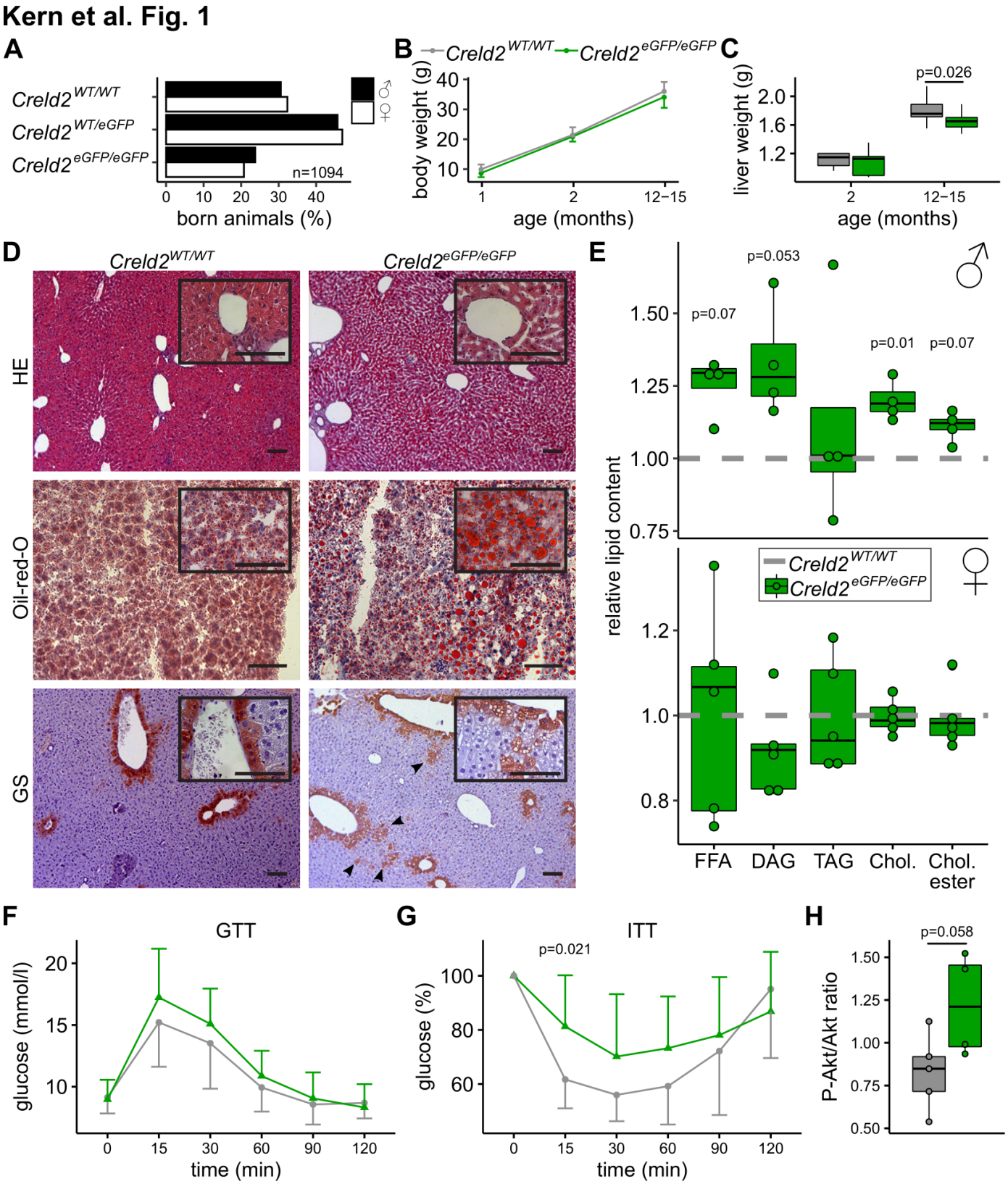

Figure 1: *Creld2*$^{eGFP/eGFP}$ males develop liver steatosis with progressing age. (A) Animals born from *Creld2* $^{WT/GFP}$ *x Creld2* $^{WT/GFP}$ matings. **(B)** Body weight of males (1 month: n = 5-7; 2 months: n = 44-50; 12-15 months: n = 18-23) **(C)** Liver weight of males (2 months: n = 5; 12-15 months: n = 11-14). Error bars represent ± SD. Unpaired two-tailed t-test. **(D)** Histological analysis of 1-year-old male livers by hemalaun and eosin (HE) (top), Oil-red-O (middle) and anti-GS (Glutamine synthetase) antibody (bottom). Arrowheads indicate ectopic GS expression. Scale bars of the overview: 100 µm. Scale bars of the insets: 10 µm. **(E)** Thin layer chromatography of total lipid extracts from 1-year-old animals (♂; n = 4, ♀; n = 3-5). Circles represent individual mice, grey lines are means of control littermates. Unpaired two-tailed t-test. **(F-G)** Glucose tolerance test (GTT, n = 9-10) (F) and insulin tolerance test (ITT, n = 8-9) of 1-year-old male mice (G). Error bars represent ± SD. Unpaired two-tailed t-test. (**H**) Ratio of phosphorylated Akt (p-Akt)/Akt expression in livers after 15 min of insulin administration in 1-year-old male mice (n = 4-5). Circles represent individual mice. Unpaired two-tailed t-test.

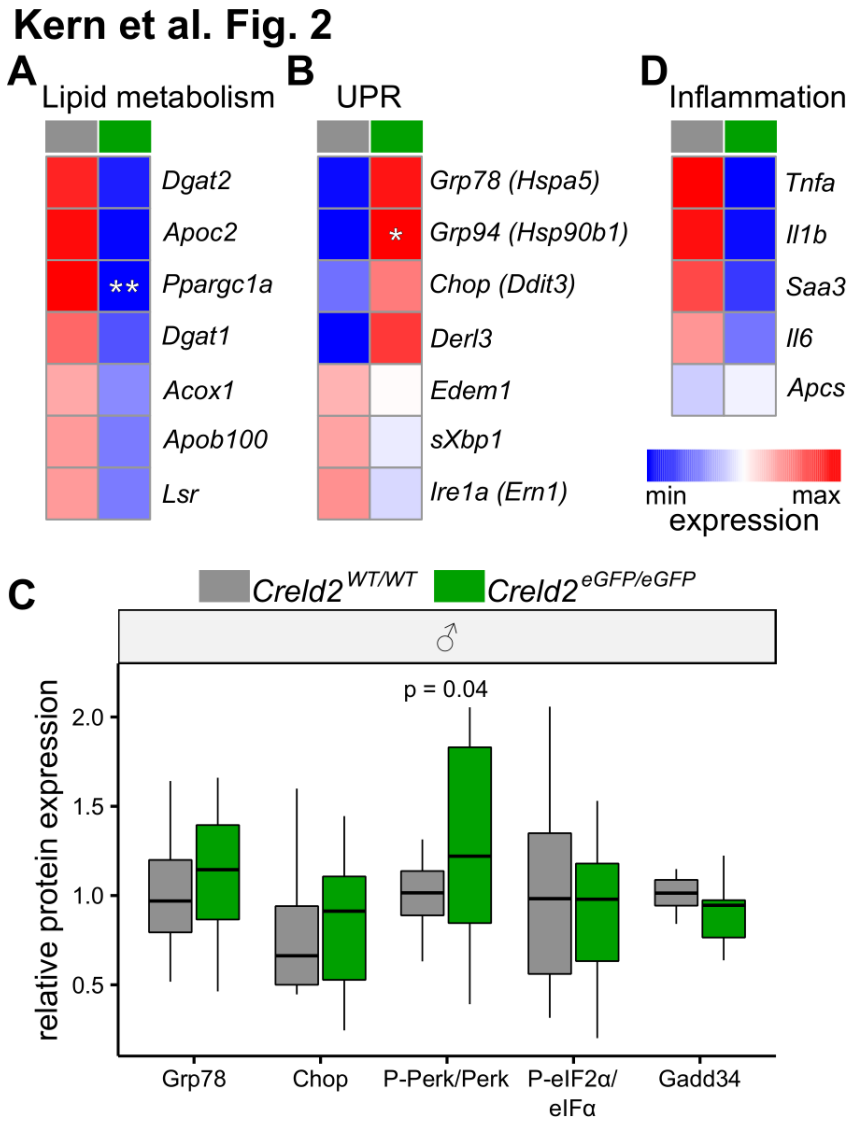

Figure 2: 1-year-old *Creld2*$^{eGFP/eGFP}$ male mice display downregulation of key lipid metabolism genes and increased ER stress marker expression. (A, B, D) qRT-PCR analysis of male livers (n = 3-5). Gene expression is displayed as relative value. Unpaired two-tailed t-test. * $p < 0.05$, ** $p < 0.01$. **(C)** Protein expression in livers of male mice as assessed by Western blot quantification (n = 17-19). For Perk and eIF2α ratios of phosphorylated (P-Perk and P-eIF2α) and unphosphorylated protein abundance are displayed.

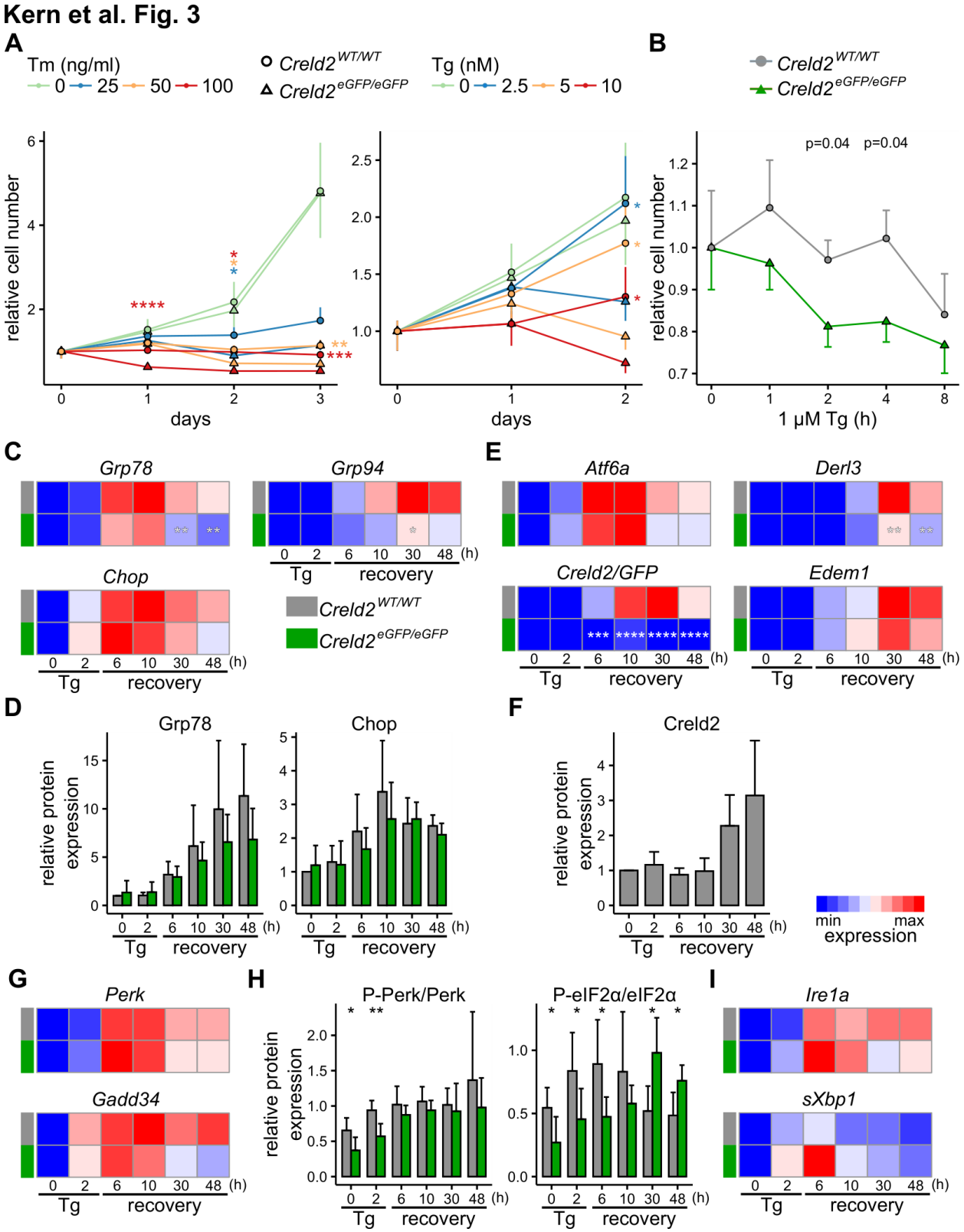

Figure 3: *Creld2*$^{eGFP/eGFP}$ mouse embryonic fibroblasts (MEFs) show reduced survival after ER stress. (A) Relative MEFs cell numbers determined by crystal violet assay after induction of chronic ER stress with various Tm (tunicamycin; up to 3 days; n = 6-16) or Tg (thapsigargin; up to 2 days; n = 13-16) doses. **(B)** Relative MEFs cell numbers determined by crystal violet assay after induction of ER stress by 1 μM Tg for up to 8 hours followed by a 5-day culture period without Tg (n = 5-8). Error bars in (A) and (B) represent ± SEM. **(C-I)** MEFs were cultured with Tg for 2 hours to induce ER stress followed by removal of Tg (hours indicate duration of experiment) to analyze the recovery capability of *Creld2*$^{eGFP/eGFP}$ cells. **(C)** qRT-PCR of the general ER stress markers *Grp78* (n = 8-10), *Grp94* (n = 3) and *Chop* (n = 8-10). **(D)** Protein expression of Grp78 (n = 7-8) and Chop (n = 3-4) assessed by Western blot. Protein expression is normalized to control at 0h. **(E)** Analysis of ATF6α-pathway components expression via qRT-PCR of *Edem1* (n = 8-10), *Derl3* (n = 8-10), *eGFP* (n = 5) and *Creld2* (n = 10). **(F)** Protein expression of Creld2 (n = 10). **(G)** qRT-PCR of *Perk* and *Gadd34* (n = 8-10). **(H)** Ratios of phosphorylated (P-Perk and P-eIF2α) and unphosphorylated Perk and P-eIF2α assessed by Western blot quantification (n = 5). **(I)** qRT-PCR analysis of *Ire1a* and s*Xbp1* (n = 8-10). Error bars in (D, F, H) represent ± SD. Gene expression (C, E, G, I) is displayed as relative value. * $p < 0.05$; ** $p < 0.01$; *** $p < 0.001$, **** $p < 0.0001$.

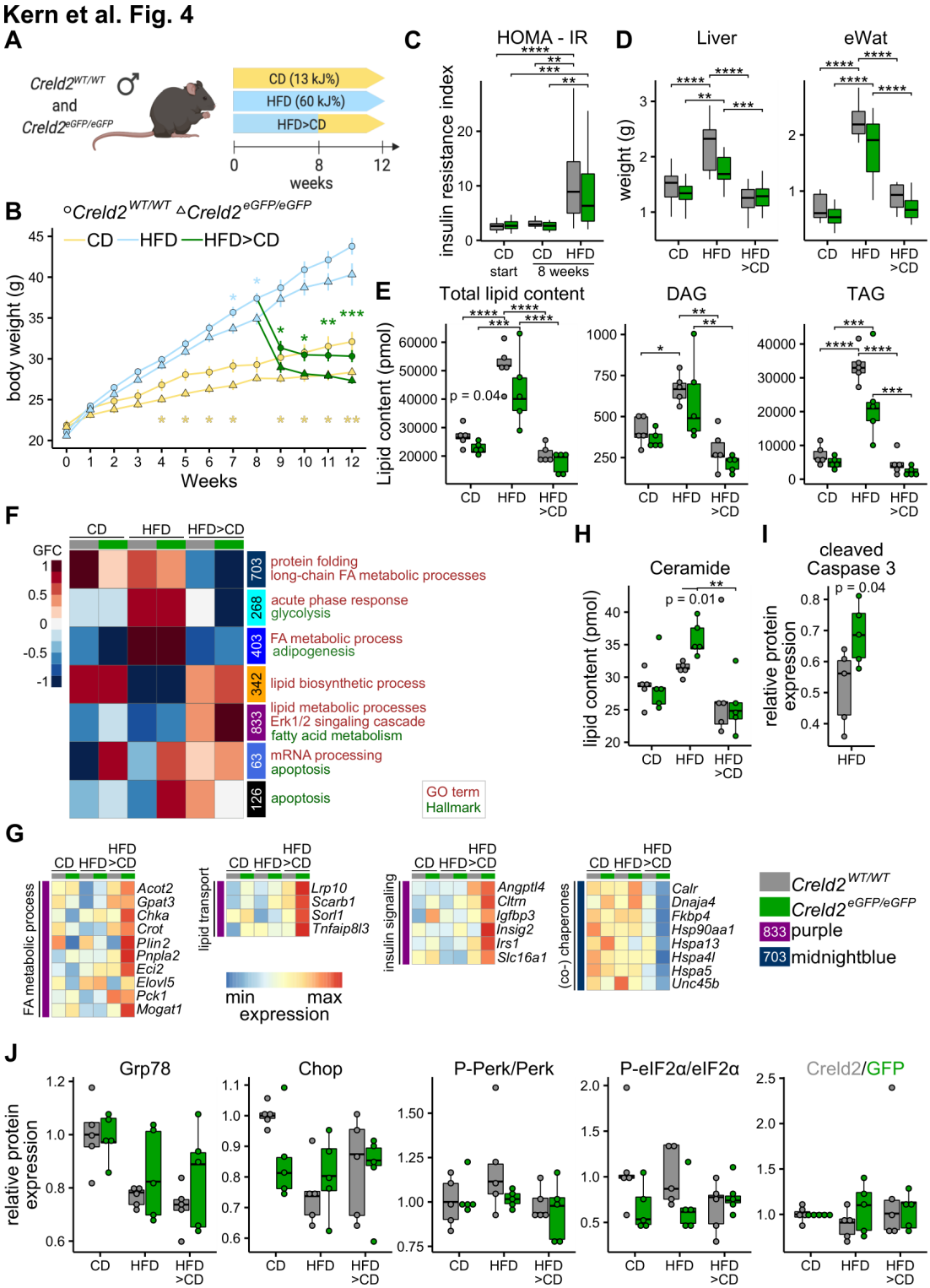

Figure 4: Tissue and molecular response of *Creld2*$^{eGFP/eGFP}$ mice to high-fat diet. (A) Experimental setup. **(B)** Body weight of male mice fed with CD (control diet; n = 13-14) and HFD (high-fat diet; n = 12-31) for 12 weeks, or HFD for 8 weeks following CD for 4 weeks (n = 14-19). **(C)** Analysis of insulin resistance induction by HFD via HOMA-IR (homeostatic model assessment of insulin resistance, CD start: n = 22-29; CD 8 weeks: n = 7-10; HDF 8 weeks: n = 17-20). One-way ANOVA with Turkey post-hoc test. **(D)** Liver (n = 12-19) and eWat (epididymal white adipose tissue, n = 9-14) weights of mice after 12 weeks of diet. **(E)** Lipid mass spectrometry of livers (n = 5). DAG: Diacylglycerol. TAG: Triacylglycerol. Circles represent individual mice. One-way ANOVA. **(F)** Co-expression network analysis (CoCena) performed on RNA-seq data of livers (n = 5 per condition). Numbers indicate genes belonging to a module. Colours represent cluster names: midnightblue: 703 genes, cyan: 268 genes, blue: 403 genes, orange: 342 genes, purple: 833 genes, royalblue: 63 genes, black: 126 genes. GFC: group fold change. **(G)** Heatmap representation of selected genes from (F), values are displayed as z scores. **(H)** Lipid mass spectrometry analysis for ceramides. Circles represent individual mice. One-way ANOVA with Turkey post-hoc test. **(I)** Western blot analysis for cleaved Caspase 3 (n = 5). Circles represent individual mice. Unpaired two-tailed t-test. **(J)** Western blot analysis for UPR components (n = 5). For Perk and eIF2α, ratios of phosphorylated (P-Perk and P-eIF2α) and unphosphorylated protein abundance are displayed. Circles represent individual mice. * $p < 0.05$; ** $p < 0.01$; *** $p < 0.001$, **** $p < 0.0001$.

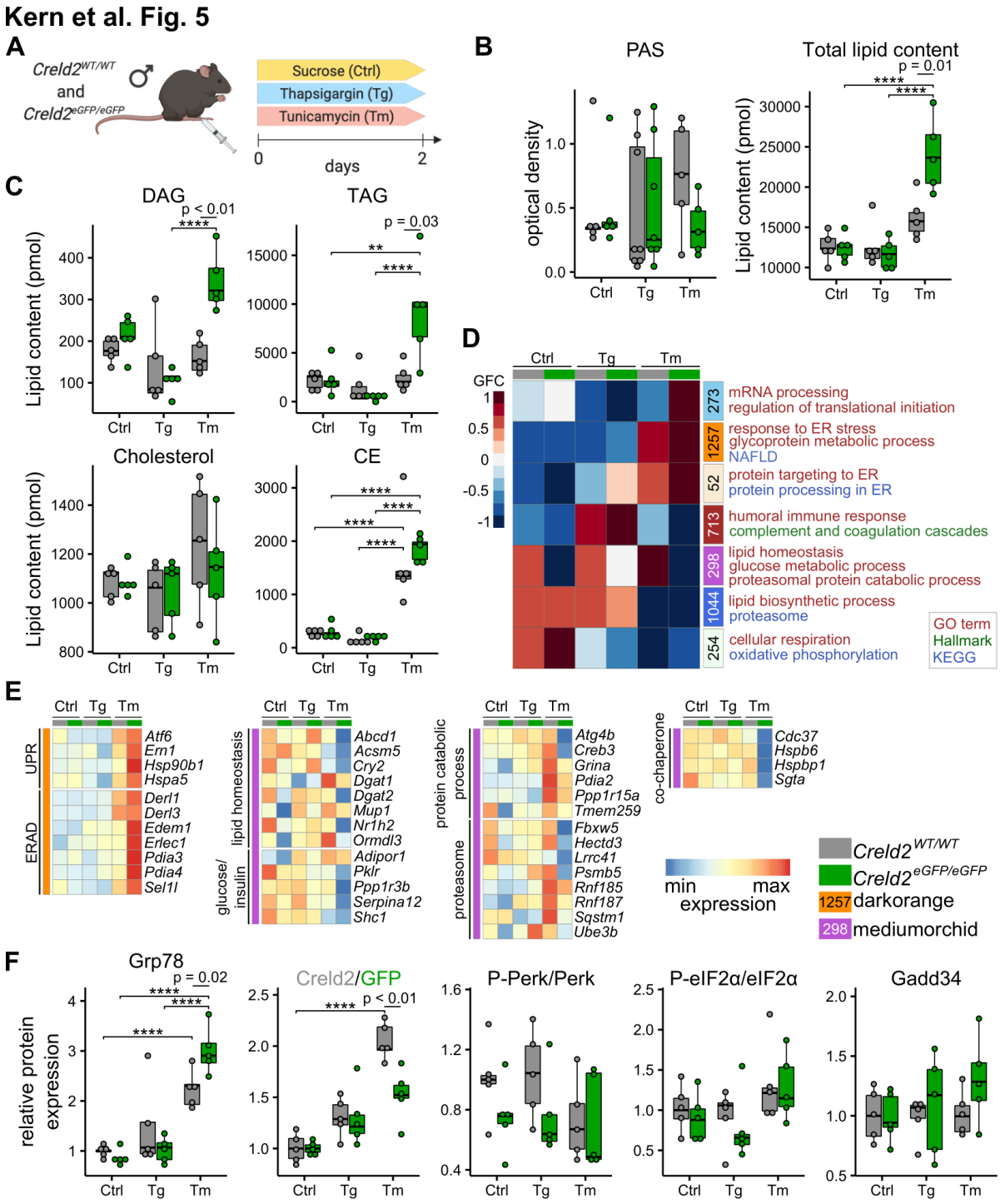

Figure 5: Tissue and molecular response of *Creld2*$^{eGFP/eGFP}$ mice to pharmacological ER stress induction. (A) Experimental setup. **(B)** Quantification of liver PAS stainings and mass spectrometrical assessment of liver lipids. Circles represent individual mice. One-way ANOVA with Turkey post-hoc test. **(C)** Elevated lipid levels are mainly attributable to accumulated DAG (diacylglicerides), TAG (triacylglycerides) and CE (cholesteryl esters). Circles represent individual mice. One-way ANOVA with Turkey post-hoc test. **(D)** Co-expression network analysis (CoCena) performed on RNA-seq data of livers (n = 5 per condition). Numbers indicate genes belonging to a module. Colours represent cluster names: skyblue: 273 genes, darkorange: 1257 genes, antiquewhite: 52 genes, brown: 713 genes, mediumorchide: 298 genes, royalblue: 1044 genes, honeydew: 254 genes. GFC: group fold change. **(E)** Heatmap representation of selected genes from (D), values are displayed as z scores. **(F)** Western blot analysis for UPR components (n = 5). For Perk and eIF2α, ratios of phosphorylated (P-Perk and P-eIF2α) and unphosphorylated protein abundance are displayed. Circles represent individual mice. One-way ANOVA with Turkey post-hoc test. * $p < 0.05$; ** $p < 0.01$; *** $p < 0.001$, **** $p < 0.0001$.

Kern et al. Fig. 6

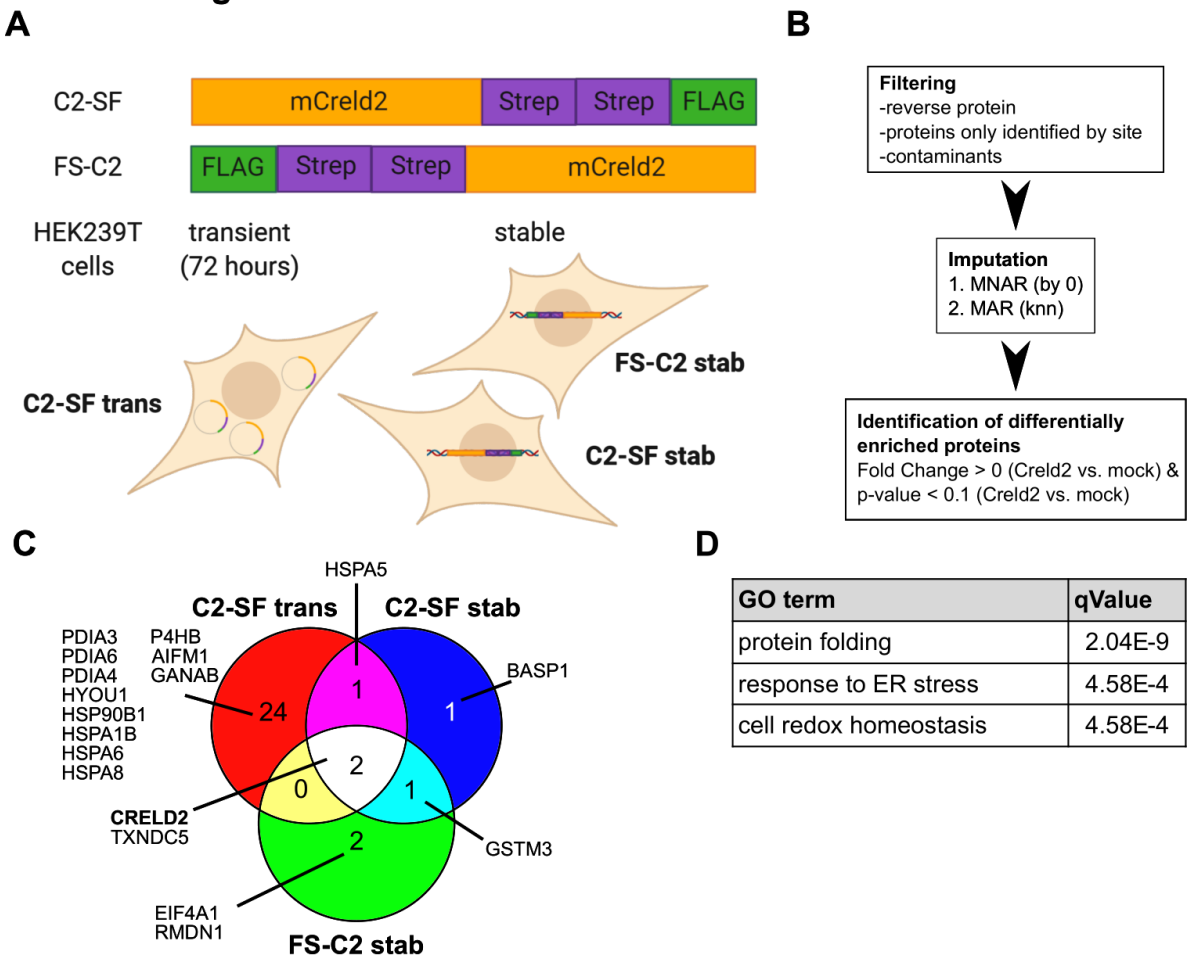

GO term	qValue
protein folding	2.04E-9
response to ER stress	4.58E-4
cell redox homeostasis	4.58E-4

Figure 6: Creld2 interacts with proteins involved in protein folding, response to ER stress and detoxification. **(A)** Schematic representation of constructs and expression conditions used for tandem-affinity-purification of tagged mouse Creld2. **(B)** Workflow chart for analysis of mass spectrometry data. knn: k-nearest neighbour; MAR: missing at random; MNAR: missing not at random. **(C)** Enriched Creld2 interaction partners across the different expression conditions. **(D)** Top three enriched GO terms resulting from enrichment analysis of all co-purified proteins.

Kern et al. Fig. 7

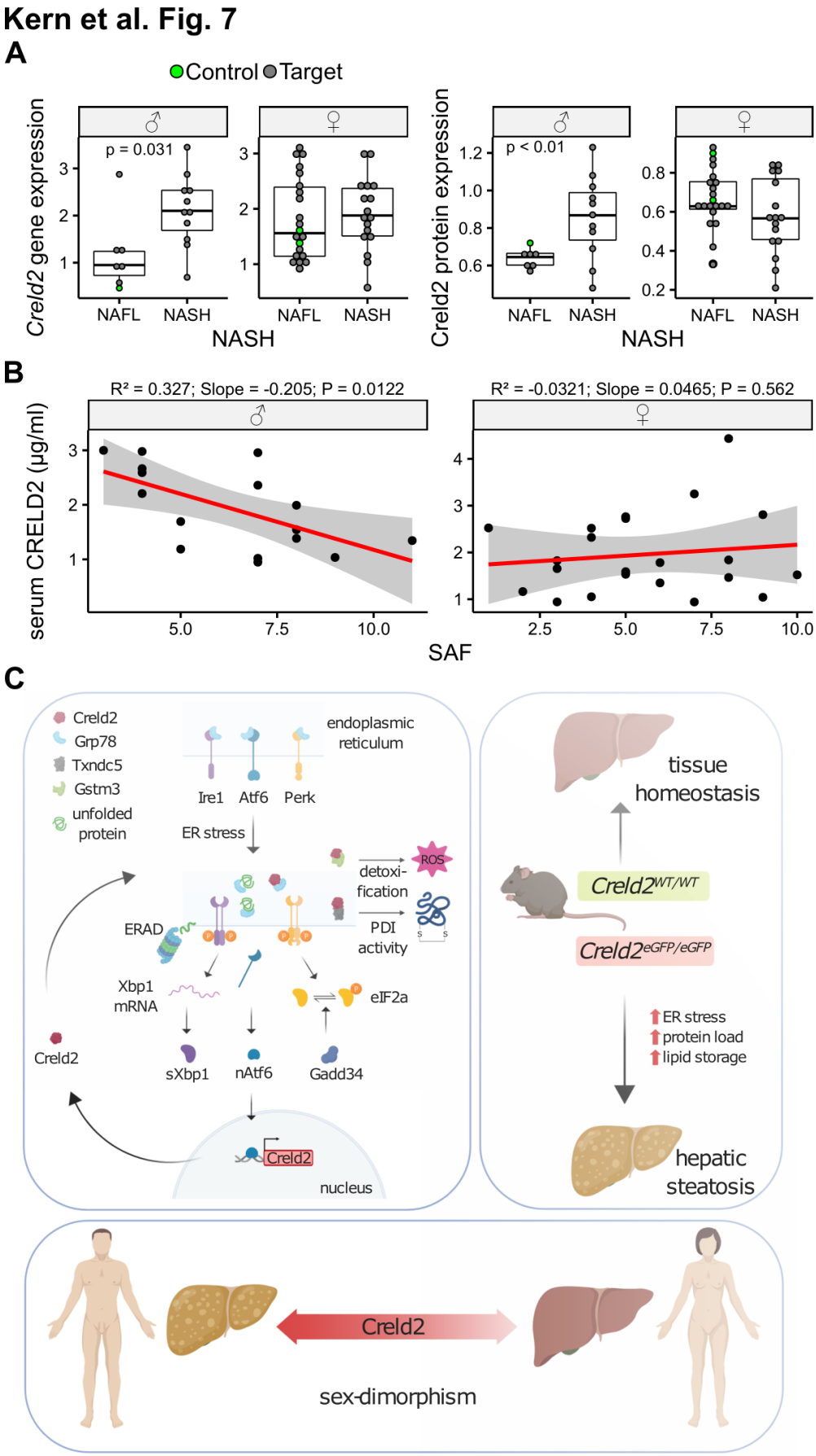

Figure 7: Hepatic CRELD2 expression increases in patients with non-alcoholic steatohepatitis. (A) Hepatic gene and protein expression levels of CRELD2 in male (♂) and female (♀) non-alcoholic fatty liver disease (NAFLD) patients (grey circles) with or without NASH (non-alcoholic steatohepatitis) and healthy controls (green circles). Cohort is comprised of 57 patients. Circles represent individual patients. Unpaired two-tailed t-test. **(B)** Analysis of CRELD2 serum concertation in male (♂) and female (♀) patients plotted against the Steatosis Activity and Fibrosis (SAF) score (cohort comprised of 40 patients). Linear regression model. Circles represent individual patients. **(C)** Summarizing schematic of Creld2 functionality. PDI: protein disulfide isomerase; ROS: reactive oxygen species.

Kern et al. Supp. 1

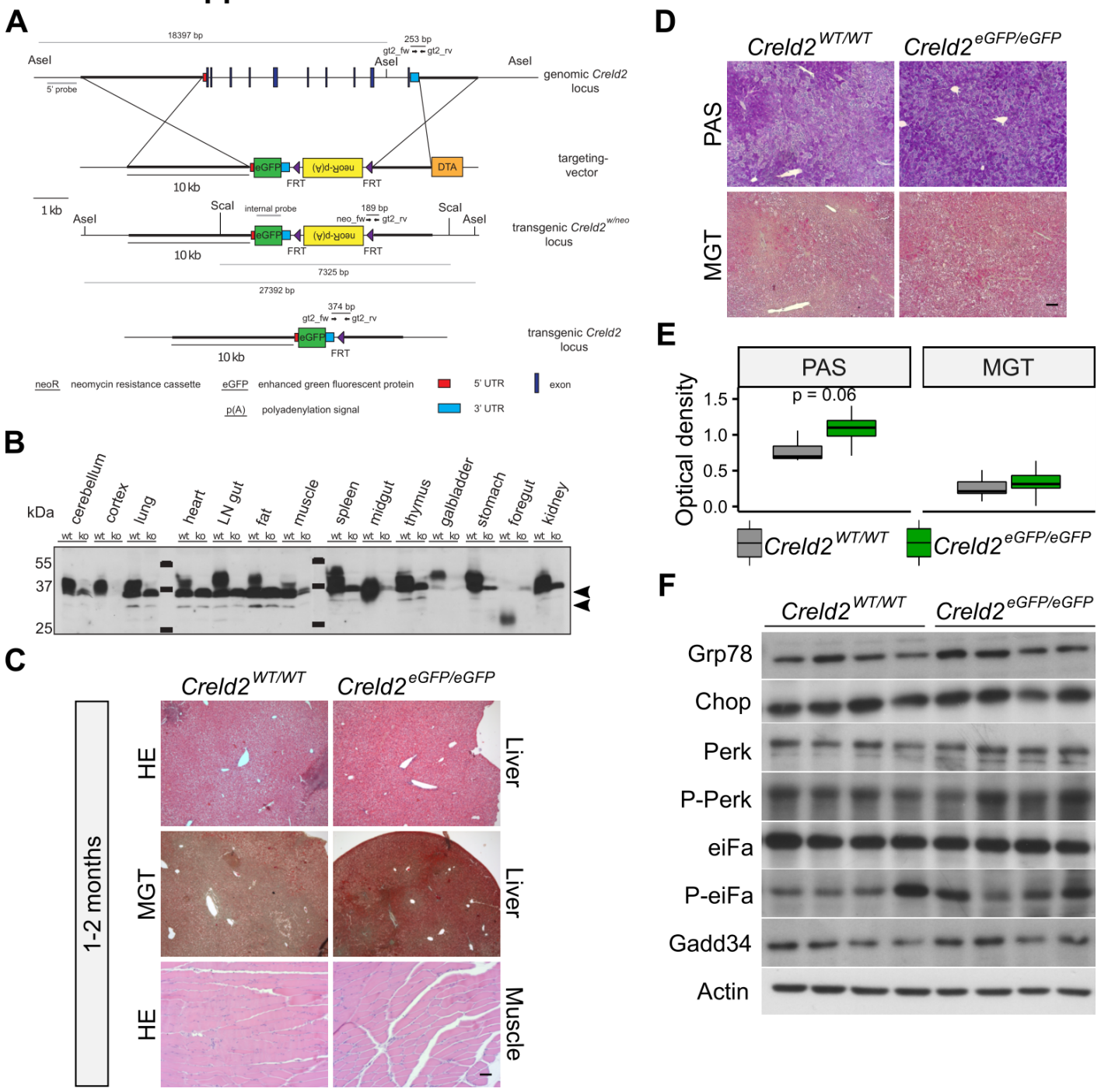

Supplemental Figure 1: Generation and phenotypic analysis of the *Creld2*$^{eGFP/eGFP}$ mouse. **(A)** Gene targeting strategy. The complete genetic locus of *Creld2* was replaced by an eGFP reporter via homologous recombination. The targeting vector comprised a neoR cassette flanked by FRT sites for positive ES cell selection. Following recombination, the neoR cassette was excised by FLP-mediated deletion. Primers for ES cell screening (gt2_fw, gt2_rv, neo_fw) and probes used for Southern blotting (5' probe, internal probe) and the resulting fragment lengths (bp) are indicated. **(B)** Tissue expression profile of Creld2 and testing of the anti-Creld2 antibody specificity by immunoblotting. Arrowheads indicate unspecific protein bands. **(C)** Histological analysis of liver and muscle tissue by hemalaun and eosin (HE) and Masson Goldner trichrome (MGT) in young *Creld2*$^{eGFP/eGFP}$ and wildtype mice. Representative for n = 8-10. **(D-E)** Representative PAS (Periodic acid Schiff) and MGT staining of 1-year-old male livers and staining evaluation (n = 11-12). Scale bar represents 100 µm. **(F)** Representative immunoblots of liver lysates from 1-year-old male mice. Refers to main Figure 2C.

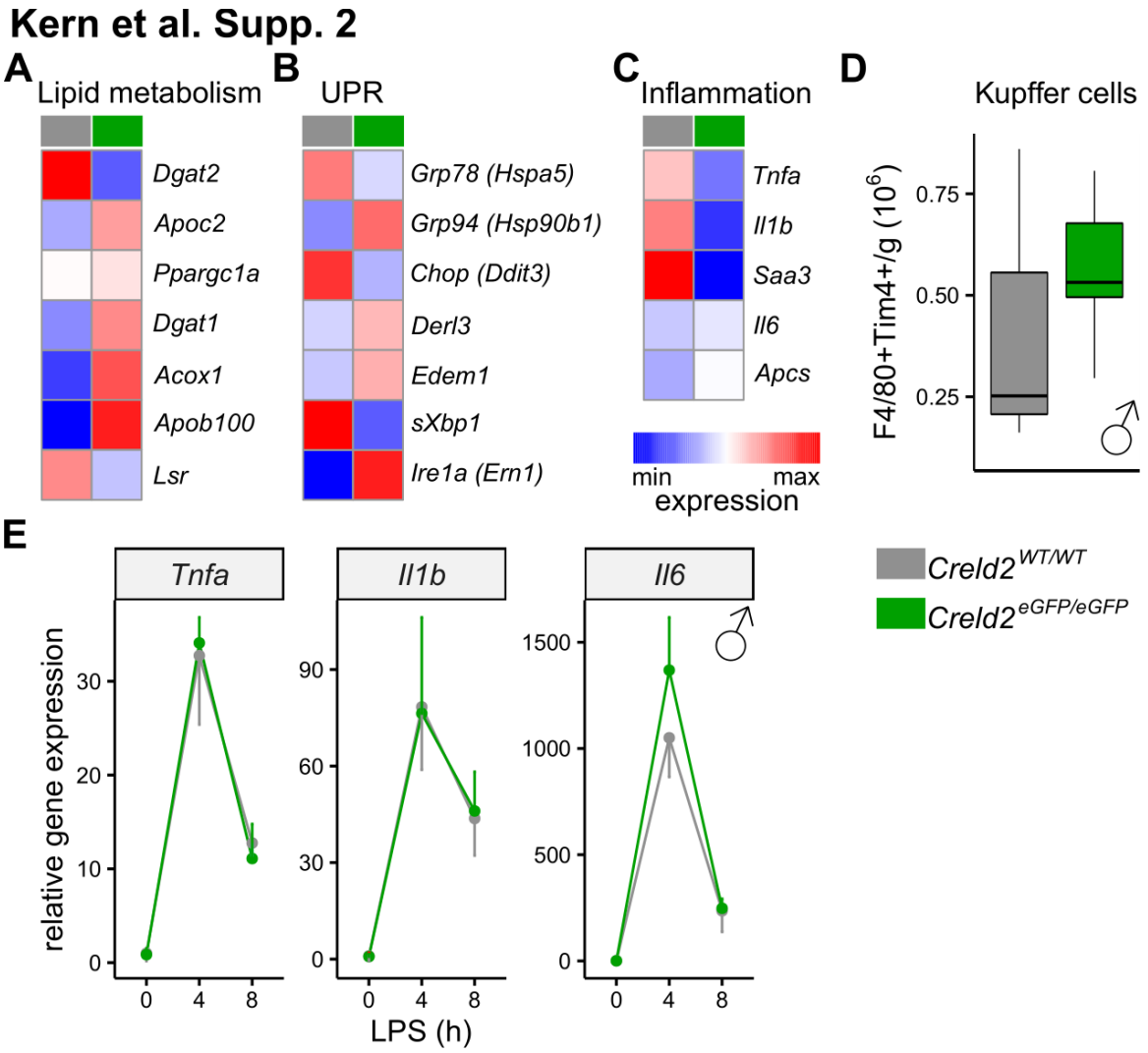

Supplemental Figure 2: Gene regulation and immune response in 1-year-old mice. (A-C) qRT-PCR analysis of 1-year-old female livers (n = 2-8). Gene expression is displayed as relative value. Unpaired two-tailed t-test. **(D)** Flow cytometry analysis of liver Kupffer cells ($CD45^{+}CD11b^{low}F4/80^{+}Tim4^{+}$) in male mice (n = 3-9). **(E)** qRT-PCR analysis of pro-inflammatory cytokines *Tnfa*, *Il1b* and *Il6* in bone-marrow derived macrophages after LPS treatment isolated from males (n = 3-4). Error bars represent ± SD.

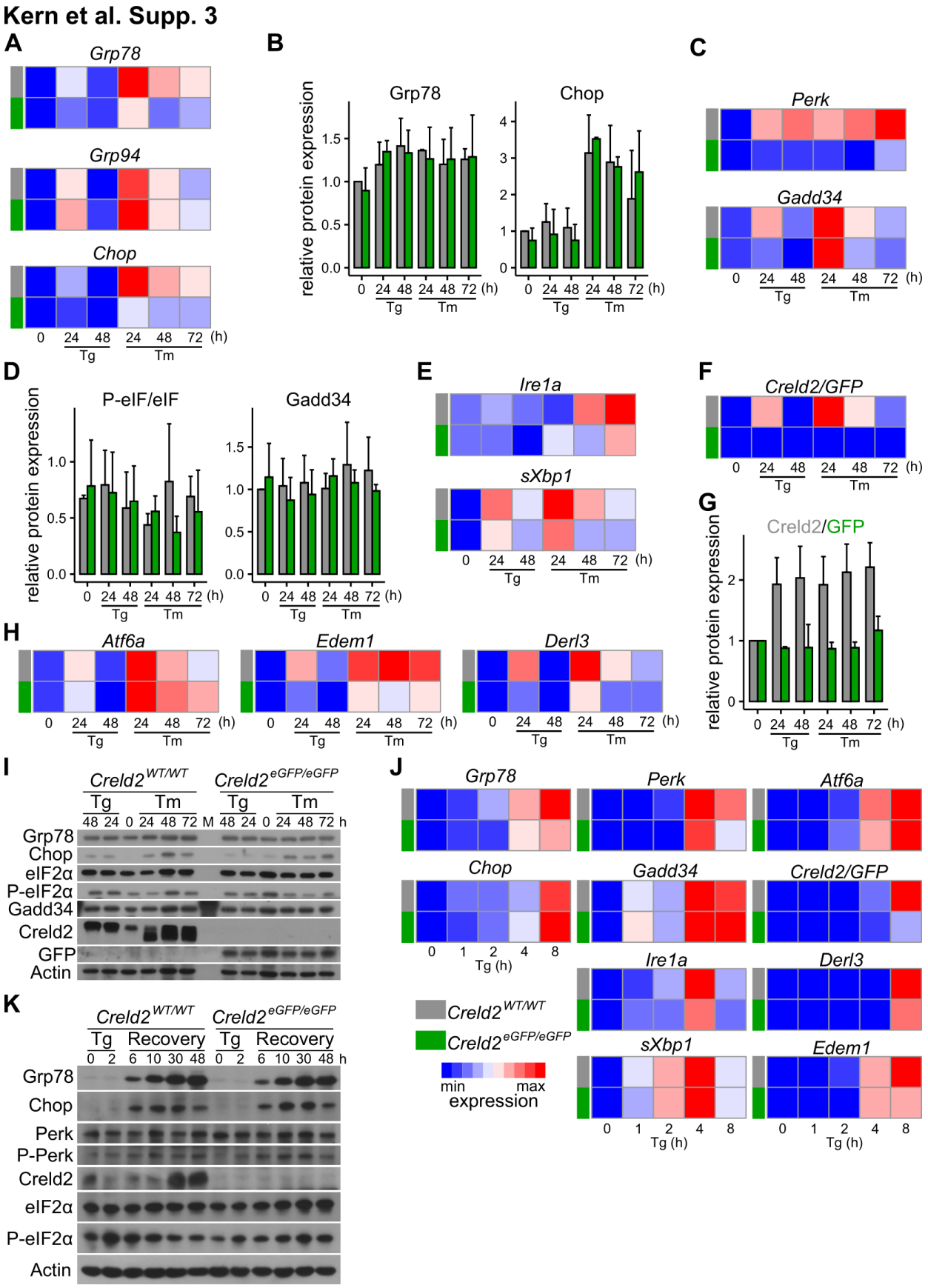

Supplemental Figure 3: *Creld2*$^{eGFP/eGFP}$ MEFs show differential responses to chronic and acute ER stress. (A-I) UPR analysis of MEFs during chronic ER stress induced by either Tg (Thapsigargin) or Tm (Tunicamycin) for up to 48 h or 72 h, respectively (n = 3)**. (A, B)** Gene (A) and protein expression analysis (B) of major ER stress makers during chronic ER stress. **(C-D)** Analysis of Perk pathway components via qRT-PCR (C) and Western blot (D). **(E)** Gene expression of *Ire1a* and *sXbp1* during chronic ER stress. **(F-H)** Analysis of Atf6 and downstream targets via qRT-PCR (F, H) and Western blot (G). **(I)** Representative immunoblots of MEFs during chronic ER stress. **(J)** Determination of the successful UPR induction by Tg (1 µM, up to 8 h) for the establishment of an *in vitro* ER stress recovery model shows upregulation of most of the monitored UPR components already after 2 h of Tg treatment (n = 2-4). **(K)** Representative immunoblots of MEFs during ER stress recovery. M: marker/ladder. Refers to main figure 3D, F, H.

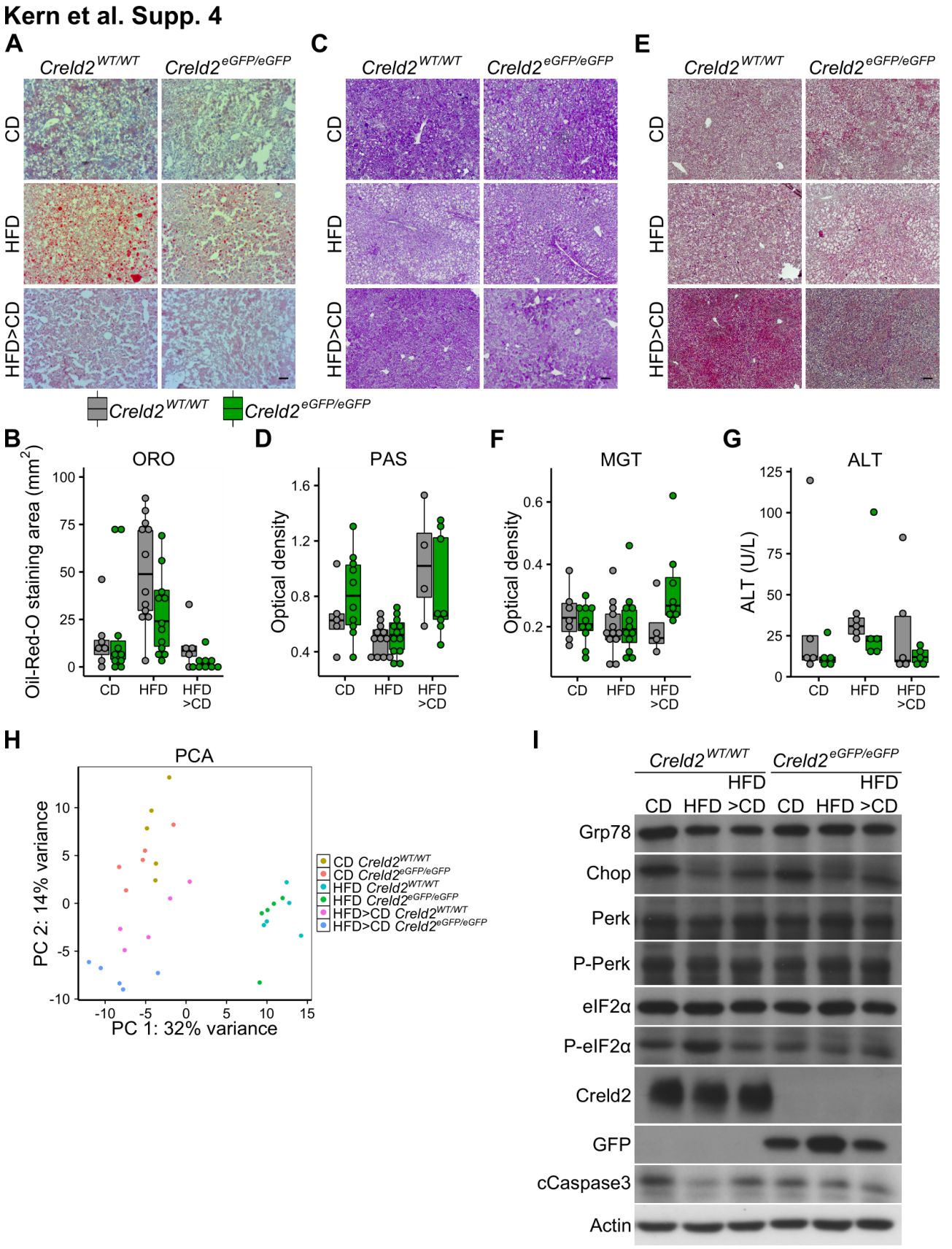

Supplemental Figure 4: Diet-induced hepatosteatosis and analysis of liver damage. (A-F) Representative histological analyses of livers from mice on different diets by (A) ORO (Oil-red-O), (C) PAS (Periodic Acid Schiff) and (E) MGT (Masson Goldner trichrome) staining and their corresponding quantification (B, D, F). **(G)** Determination of liver damage by serum alanine aminotransferase (ALT) concentration. Circles represent individual mice (B, D, F). Scale bars represent 100 µm. **(H)** Principle component analysis of liver RNA-seq data shown in Figure 4. **(I)** Representative immunoblots of liver protein lysates on different diets. Refers to main Figure 4J.

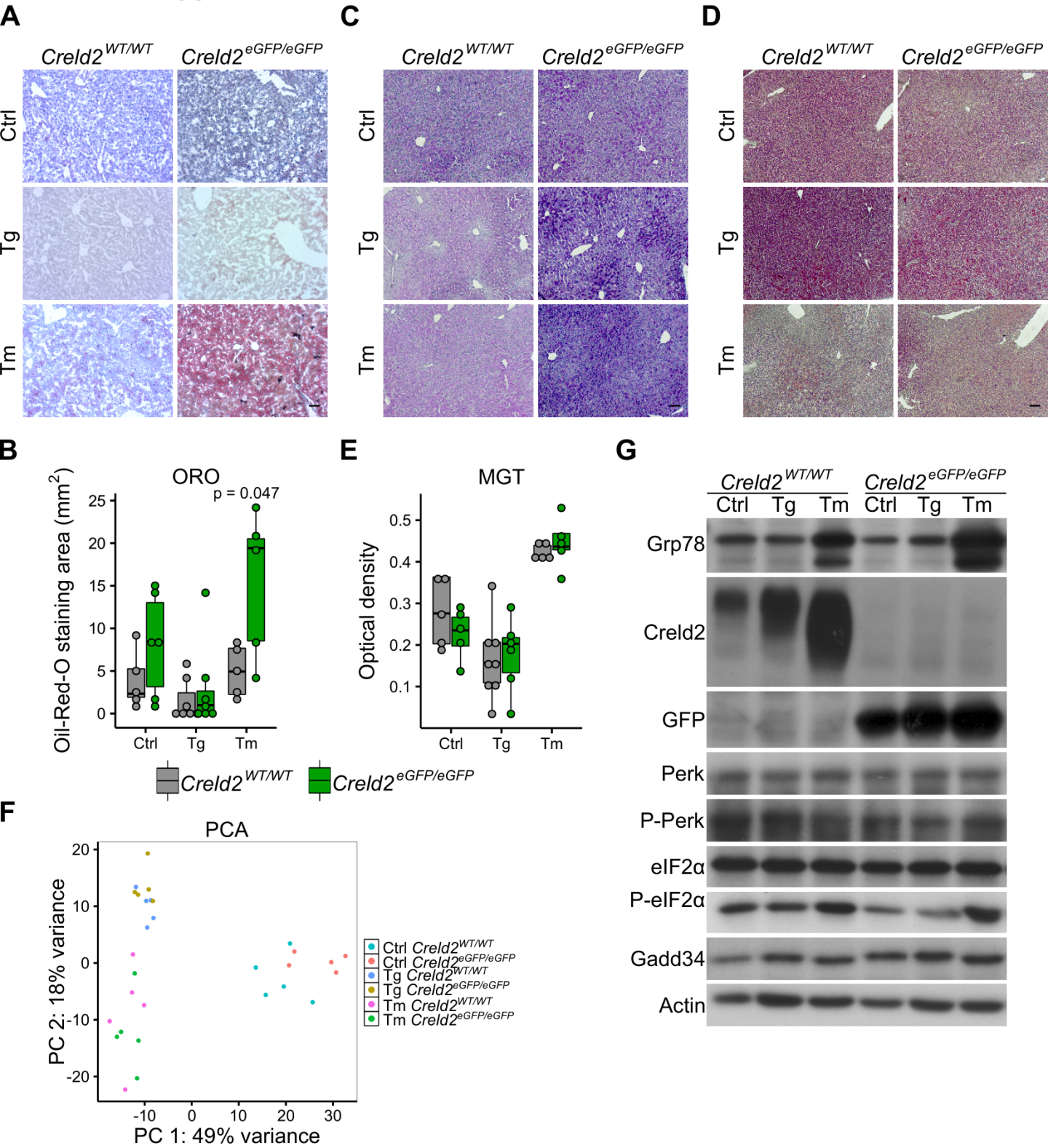

Supplemental Figure 5: Pharmacologically induced hepatosteatosis and analysis of liver damage. (A) ORO (Oil-red-O) staining of livers from ER stress induced mice (Ctrl: Sucrose control; Tg: Thapsigargin; Tm: Tunicamycin) and **(B)** ORO staining quantification. **(C)** PAS (Periodic Acid Schiff) staining. For PAS signal intensity quantification see Figure 5B. **(D, E)** MGT (Masson Goldner trichrome) staining and quantification. Circles represent individual mice (B, E). Scale bars represent 100 µm. **(F)** Principle component analysis of liver RNA-seq data shown in Figure 5. **(G)** Representative immunoblots of liver protein lysates injected with sucrose control (Ctrl), Tg (thapsigargin) or Tm (tunicamysin). Refers to main Figure 5F.